d'Collection

A THESIS
FOR THE DEGREE OF MASTER OF SCIENCE

Fucosterol and alginic acid purified from *Padina commersonii* from the Maldives; inhibit particulate matter induced inflammation through NF-κB, MAPK mediated inflammatory pathway and oxidative stress via Nrf2/HO-1 pathway

THILINA U. JAYAWARDENA

Department of Marine Life Sciences

GRADUATE SCHOOL

JEJU NATIONAL UNIVERSITY

August, 2019

Fucosterol and alginic acid purified from *Padina commersonii* from the Maldives; inhibit particulate matter induced inflammation through NF-κB, MAPK mediated inflammatory pathway and oxidative stress via Nrf2/HO-1 pathway

Thilina U. Jayawardena

(Supervised by Professor You-Jin Jeon)

A thesis submitted in partial fulfilment of the requirement for the degree of

Master of Science
August 2019

The thesis has been examined and approved by
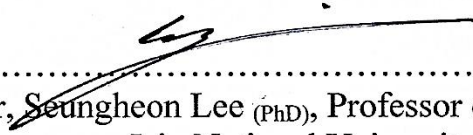
....
Thesis director, Seungheon Lee (PhD), Professor of Marine life Sciences, Jeju National University

....
K.K. Asanka Sanjeewa (PhD), Postdoctoral Researcher of Marine life Sciences, Jeju National University
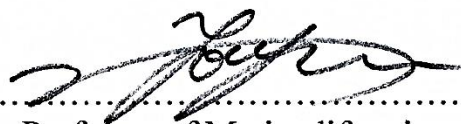
....
You-Jin Jeon(PhD), Professor of Marine life sciences, Jeju National University

2019/8
Date

Department of Marine Life Sciences
GRADUATE SCHOOL
JEJU NATIONAL UNIVERSITY

Contents

Summary

Bioactive components from marine algae have provided new insights to the natural product research. The study was concentrated on the marine brown algae *Padina commersonii*; prominent species in the Laccadive Sea. Particulate matter (PM) was associated with the study as it's considered to be a significant participant in the air pollution and hence an inducer in serious health issues. Particulate matter which is airborne due to natural sources is combined with anthropogenic sources such as industrial and traffic emissions. PM causes asthma, lung tissue damage as well as inflammation and oxidative stress.

The first part of the study focuses on the isolation of fucosterol and evaluation of its potential to attenuate inflammatory responses. Fucosterol was isolated through successive open silica columns and was characterized via GC-MS and FT-NMR. The study discovered the resilient anti-inflammatory potential via the down-regulation of nitric oxide (NO) levels in PM stimulated RAW 264.7 macrophages. Continued studies revealed its ability to abate the activity of pro-inflammatory cytokines (IL-1β, IL-6, TNF-α) including PGE_2. Gene expression studies via q-PCR and western blot analysis of the iNOS and COX-2 supported the above. Further, the mediation of the responses was evident to be activated through nuclear factor κB (NF-κB) and mitogen-activated protein kinase (MAPK) pathways. The Nrf2/HO-1 studies solidified the interconnection between inflammation and oxidative stress. Hence, the first part exposed the ability of fucosterol to successfully down-regulate the inflammatory responses stimulated via PM in RAW 264.7 macrophages.

Alginic acid was purified in the second part of the study. The protective effect of alginate from *Padina commersonii* (PCA) against PM was evaluated. In between the

external and internal environments, skin is considered to be more than a physical barrier. A crucial role of the skin is to provide immune functions. It is suggested to function as a semiautonomous immunological organ. As the keratinocytes are the outermost layer of the skin, it is regularly used to assess the effect of the irritants in the dermatology. These cells participate in immune responses via the production of cytokines against the inflammatory events. It was observed that PM stimulate inflammation in HaCaT keratinocytes and in the dermal fibroblasts (HDF) inducing inflammatory pathways. PCA was evident to act as an active protector of the PM and to down-regulate the pro-inflammatory cytokines and inflammatory mediators. Further, certain key molecules in the NF-κB and MAPK pathways in the cells were studied. The activation of the above was inhibited via the activity of PCA. The metal ion content of PM was considerably reduced by PCA and thus attributed to its chelation ability. Hence, PCA is a potent protector against PM-induced inflammation in skin damage.

Concisely, results suggest the bioactive components derived from the brown algae *Padina commersonii* increases the cellular resistance to PM stimulated inflammation and oxidative stress.

Keywords: *Padina commersonii*; MAPK; NF-κB; Nrf2/HO-1

List of figures

List of Tables

PART I

Fucosterol isolated from *Padina commersonii*, inhibits particulate matter-induced inflammation through NF-κB, MAPK mediated inflammatory pathway and oxidative stress via Nrf2/HO-1 pathway in RAW 264.7 macrophages

1.1. Introduction

The destruction of the ecological environment is contributed with various factors such as biological hazard waste, chemical waste. Over the past decade ambient air pollution through vehicle emission dust and industrial emissions has increased. It was reported that the air pollution as the world's largest single environmental health risk [1]. The airborne particulate (PM) matter is associated with various health risks including respiratory disorders, allergic reactions, cardiovascular diseases and dermal diseases. PM has become a major concern globally, in particular in the East Asia region including China, Korea and Japan. It's considered, Beijing as a heavily air polluted city in the world [2]. Though the anthropogenic sources are contributing towards this, a major natural contributor is the particulate matter originate during the spring season in Loess Plateau, desert regions of Mongolia, and northwest China. Lee et al (2015) reported, emissions released by China are much smaller compared with non-anthropogenic sources [3].

PM is a complex mixture of biological materials (pollen, micro-organisms), metallic ions, organic matter and poly-aromatic hydrocarbons. The inorganic composition of fine dust was characterized by Maxwell et al. (2004) using Asian dust and the main components were reported as water-soluble mineral dust are Mg^{2+} and Ca^{2+}. Further, fine-particle negative ions remain as nitrate (NO_3^-) and sulfate (SO_4^{2-}) associated with ammonium (NH_4^+) or potassium (K^+) [4]. Factors which influence the toxicity of PM was reported by Harrison and Yin (2000), as bulk chemical composition, trace element content, strong acid content, sulfate content, and particle size distribution [5]. Lv et al (2016), analysed systematically the PM 2.5 Beijing urban fine dust and its sources descriptively with environmental impacts [6]. Particulate matter is generally consisted of coarse and fine fractions. The coarse fraction is consisted mainly of natural

sources such as re-suspended dust and biological material (pollen, bacteria). Whereas fine particles which are less than 2.5 µm is dominated by anthropogenic emissions [7].

Earlier reports indicate that the metal content and its acidity specifically transition metals interfering with host defence mechanism and cause of inflammation [8, 9]. The PM pollution in vitro studies have exhibited cytotoxicity, oxygen radical formation and cytokine release signifying the effect of particulate pollution in inflammatory disorders [10, 11]. Shukla et al (1999), reported on the effect of the fine particulate matter inhalation and NF-κB related inflammatory activation in pulmonary epithelial cells [12]. Similarly, Zhao et al (2016) reported on the effect of fine dust in inflammatory pathway activation through ROS-dependent mechanisms [13]. ROS plays an important role in the elimination of microbes inside the lungs. Though the over production of ROS results in oxidative stress. Due reason live cells are damaged leading to internal disorders. Respiratory diseases, excessive inflammation and oxidative stress are reported as the major causes [14, 15].

The lifespan of marine algae are exposed to extreme conditions. It faces high oxygen concentrations, intense light, UV radiation, and stress. Due to its richness with bioactive components, the stressful conditions could overcome successfully [16]. Earlier reports indicate the focus of different bioactive components form brown algae such as fucoxanthin [16], chromenes [17], and diphlorethohydroxycarmalol [18].

Padina commersonii/ boryana is a brown algae specie widespread in warm Indo-pacific waters. This has been exposed to studies in several occasions. Fernando et al (2018), used the carbohydrase assisted extraction for *P. commersonii* and evaluated its anti-oxidant and anti-inflammatory potentials briefly [19]. Fucoidan from this species has been widely studied for its structure and anticancer activity by Usoltseva et al (2017) [20].

Fucosterol is phytosterol, apparently abundant in brown algae and was first identified in its pure form by Heilbron et al. (1934) publishing an article highlighting its potentials [21]. Varying aptitudes of it has been reported vividly in different occasions. Antioxidant effects of fucosterol was reported using *Pelvetia siliquosa* [22]. Its anti-inflammatory properties against LPS stimulated conditions were earlier reported by Jung et al (2013) using brown algae *Elsenia bicyclis* [23]. The anti-osteoporotic effect was evaluated using fucosterol derived from *Undaria pinnatifida* [24]. Fernando et al (2019), studied and reported on the potential of fucosterol to inhibit particulate matter induced inflammation and oxidative stress in the alveolar cell line A549 [25].

This study aimed to isolate fucosterol form brown algae *P. commersonii* and to evaluate its anti-inflammatory properties on the PM induced RAW 264.7 macrophages. Pure compound fucosterol identification was assisted by the NMR spectroscopy (nuclear magnetic resonance) and GC-MS (gas chromatography-mass spectroscopy) data. The preliminary studies revealed its potential to inhibit PM induced inflammation. Hence, further studies were conducted to confirm its activity using RT-qPCR techniques for gene expression analysis and western blotting as well as ELISA techniques. The activity was anticipated to be occurred via the MAPK and NF-κB pathways. Further we have elevated our studies to the level of oxidative stress related protein expression analysis. To the best of our knowledge, this is the first report with regard to the assessment of fucosterol on the particulate matter induced inflammation in RAW 264.7 macrophages.

1.2. Methods

1.2.1 Materials

Certified reference material No. 28; China fine dust particulate matter (PM) was purchased from the National Institute for Environmental Studies, Ibaraki, Japan. All the organic solvents (HPLC grade) used in the experiments were purchased from Sigma-Aldrich (St Louis, MO, USA). Silica gel 60 F254 TLC plates were purchased from Merck (Darmstadt, Germany). Silica (30–60 mesh), for open column preparation was from Sigma-Aldrich. Deuterated chloroform for NMR analysis was obtained from Cambridge Isotope Laboratories (Andover, MA, USA). RAW 264.7 macrophage cell line was purchased from the Korean Cell line Bank (KCLB, Seoul, Korea). Dulbecco's modified Eagle's medium (DMEM), fetal bovine serum (FBS), and antibiotics (penicillin and streptomycin) for growth medium were purchased from the GIBCO Inc. (Grand Island, NY, USA). 3-(4,5-dimethylthiazol-2-yl)-2,5-diphenyltetrazolium bromide (MTT), were purchased from Sigma-Aldrich. The cytokine kits used in the experiments were purchased from eBioscience (San Diego, CA, USA), R&D Systems (Minneapolis, MN, USA), BD Opteia (San Diego, CA, USA), and Invitrogen (Carlsbad, CA, USA). Western blotting antibodies were purchased from Santa Cruz Biotechnology (Ca, USA).

1.2.2 Collection of samples, extraction and isolation of fucosterol

P. commersonii samples were collected from the Fulhadhoo island coastal area of the Maldives in January 2018. Samples were immediately washed with running water to remove epiphytes and sand. The samples were then freeze dried and powdered. Sample repositories were stored in the Marine bio resource technology lab, Jeju National University. Sample extraction was conducted successfully with 70% ethanol for four times. This was evaporated to obtain the crude ethanolic extract of *P. commersonii* (PCE).

PCE was dissolved in deionized water and fractionated successively using hexane, chloroform and ethyl acetate. Using a silica open column, the hexane fraction (PCEH) was further resolved into five fractions (PCEH1-PCEH5). The elution solvent was consisted of hexane and ethyl acetate as increasing polarity (9:1→7:3→1:1)→ethyl acetate, and ethyl acetate: methanol (1:1). Fraction PCEH2 was further resolved via a second open column. The elution was done in the same solvent system with increasing polarity (85:15→7:3→1:1 and ethyl acetate). This resulted in four fractions (PCEH21-PCEH22). The PCEH22 was finally resolved in a long silica open column resulting a collection of 96 tubes. This was analysed by TLC and the tubes were pooled into four fraction (F1-F4). Fraction F2 was resolved via preparative TLC resulting 7 fractions (F2A-F2G). Among these fraction F2F indicated the presence of fucosterol (FST) and was identified as the active metabolite. Figure 1.1 indicate the detailed purification and isolation procedure. The sample was used for cell culture bioassays after dissolving in DMSO and successful serial dilution in culture media. The sample DMSO concentration in working samples were maintained less than 0.1% [26].
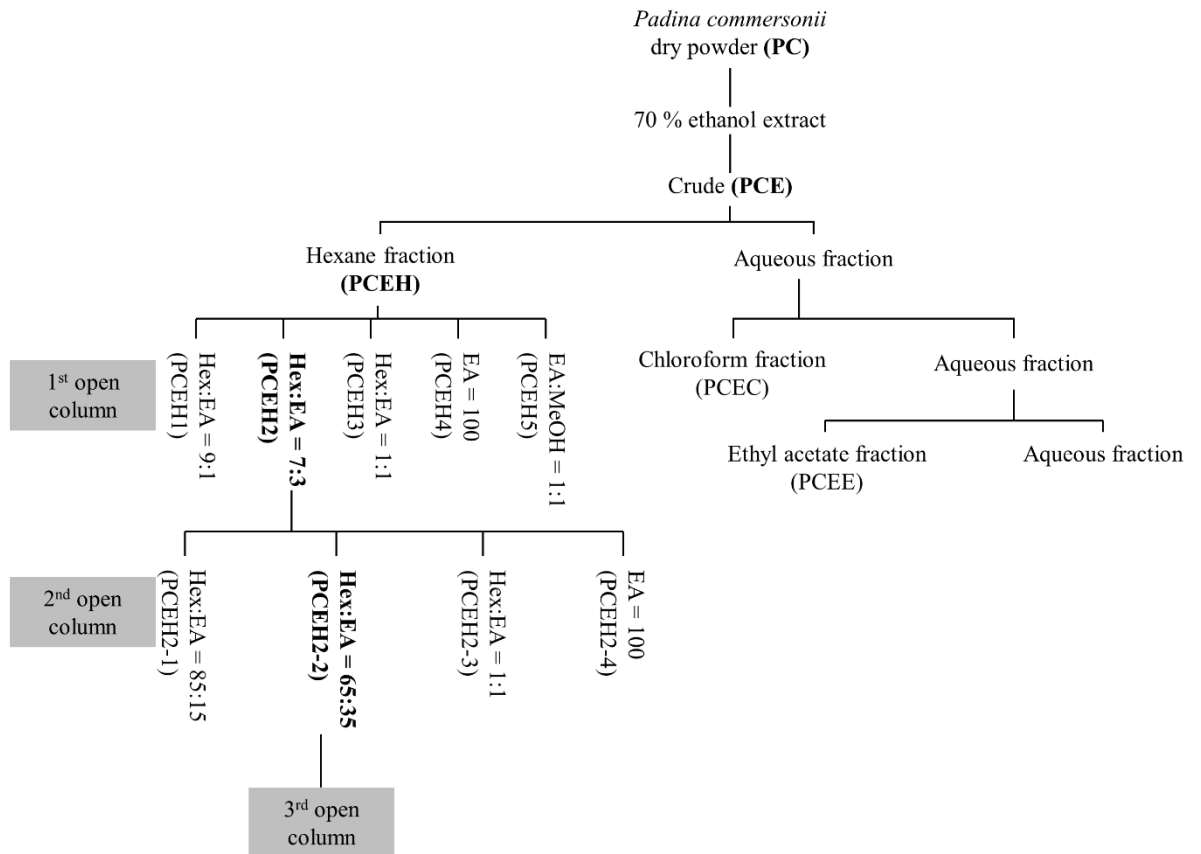
Figure 1. 1. Flow diagram representing the extraction and fractionation of *Padina commersonii* 70% ethanol extract (PCE).

1.2.3 Fucosterol structure elucidation and characterization

Fucosterol structure was confirmed by GC-MS analysis (Shimadzu GCMS-TQ8040, Shimadzu corp., Kyoto, Japan). Method involved a fused silica capillary column (RTx-5MS, 30 m×0.25 mm i.d., 0.25 µm film thickness). Injection temperature 280 ℃, and injected via splitless mode. Oven program as 260 ℃, 3 min, 6 ℃/min to 320 ℃, 5 ℃/min to 330 ℃, 2 min. The ion source temperature was maintained at 200 ℃. The scan range was 50-500 m/z. Helium was used as the carrier gas with a constant flow rate of 0.73 mL/min [27].

Nuclear magnetic resonance spectroscopy (NMR) was conducted using a 400-MHz spectrometer (JNM-ECX400, JEOL, Japan). ^{1}H and ^{13}C NMR spectra were successfully obtained. Sample was prepared by dissolving minute amount in $CDCl_3$. The chemical shifts are demonstrated in ppm while the coupling constants in Hz. Multiplicity abbreviations are used as following; s = singlet, d = doublet, t = triplet, dt =doublet of triplet, dd = doublet of doublet and m = multiplet. Heteronuclear single quantum coherence (HSQC) and heteronuclear multiple bond correlation (HMBC) was conducted to confirm the carbon multiplicity and carbon positons correlated to protons [26, 28].

1.2.4 Fine dust particle size estimation using SEM

The FD specimen was initially sputter coated with platinum. A Q150R rotary-pumped sputter coater (Quorum Technologies, Lewes, UK) was utilized for the purpose. The surface morphology of the CRM No. 28 particles were observed using a JSM-6700F field-emission scanning electron microscope (JEOL, Tokyo, Japan). The instrument was operated at 10.0 kV.

1.2.5 Cell culture

RAW 264.7 macrophage cell line was maintained in the DMEM medium which was supplemented with 10% FBS and 1% antibiotics. The cells were maintained under controlled conditions as 5% CO_2 level and 37°C temperature. The cells were periodically subcultured and used for experiments in its exponential growth phase.

1.2.6 Measurement of cell viability

The cytotoxicity against CPM-stimulated macrophages with initial fraction and purified compound FST was performed using MTT assay [29]. Once the cells reached its exponential growth phase seeding was done with a cell concentration of 1×10^5 cells mL^{-1}. FST was treated after a 24h incubation period. PM (125 µg mL^{-1}) was treated after 1h and continued its incubation further for 23h. The assay results were obtained in the 540 nm optical density value. In each step of purification, this experiment was performed and subsequent experiments were planned depending on the results.

1.2.7 Evaluation of NO inhibition activity

The macrophage cell line was seeded in a similar manner to the MTT assay. The samples were treated and was incubated for 1 h and was stimulated with PM. A 23 h further incubation was continued. NO production analysis was done using the Griess assay [30, 31]. The NO production inhibition of each sample was evaluated as a ratio of the cells exposed to LPS or PM. In each step of purification, this experiment was performed and subsequent experiments were planned depending on the results.

1.2.8 Assessing PGE$_2$ and pro-inflammatory cytokine production

The cells were seeded and treated with different concentrations of FST and was co-treated with PM (125 µg mL^{-1}). After a complete incubation period, the cell media was retrieved and was used for the analysis of each parameter expression levels. The PGE$_2$, IL-1β, IL-6, and TNF-α levels were analyzed separately using commercial cytokine analysis kits following the manufactures instructions.

1.2.9 Western blot analysis

Western blot analysis was used to measure the protein levels of iNOS, COX-2, NF-κB pathway proteins (p50 and p65 total and phosphorylated forms in nucleus and cytoplasm), MAPK pathway proteins (p38, ERK, and JNK total and phosphorylated forms), and oxidative stress related proteins (Nrf2, Keap1, and HO-1 in both nucleus and cytoplasm). 6 well culture plates were used for cell seeding with a cell concentration of 2×10^5 cells mL^{-1}. FST was treated and the cells were stimulated with PM and was incubated for another 23h. Depending on the protein type of analysis, cell harvesting was performed in two different intervals. For the analysis of NF-κB, MAPK pathway protein expression levels, and oxidative stress related proteins, the cells were harvested within 20 minutes of PM stimulation, whereas for the iNOS and COX-2 after 23h of PM stimulation. Ice-cold PBS was used to wash the harvested cells and was lysed using a Nuclear and cytoplasmic protein extraction kit (NE-PER®, Thermo Scientific, Rockford, USA). Each extract protein level was measured using BCA protein assay kit and was standardized (Bio-Rad, USA). Electrophoresis was carried out using sodium sulfate-polyacrylamide gels (12%). Subsequently, transferred onto nitrocellulose membranes. The membranes were blocked with skim milk and was incubated overnight with relevant primary antibodies (iNOS, COX-2, p50, p-p50, p65, p-p65, p38, p-p38, ERK1/2, p-ERK1/2, JNK, pJNK, Nrf-2, Keap1, and HO-1) (Santa Cruz Biotechnology) in 5% skim milk.

Following the HRP-conjugated secondary antibodies were added to the membranes and was incubated. Finally, the bands were developed using chemiluminescent substrate (Cyanagen Srl, Bologna, Italy), and was photographed using a FUSION SOLO Vilber Lourmat system. The band intensities were quantified using the ImageJ program [31, 32].

1.2.10 Extraction of RNA and cDNA synthesis

After successive cell seeding and sample treatment the total RNA from RAW 264.7 cells were extracted using a Tri-Reagent™ extraction kit (Sigma-Aldrich, St. Louis, MO, USA). During the extraction the manufactures instructions were followed. Using a μDrop Plate (Thermo Scientific) the purity of the extracted RNA was measured. With the purpose of synthesizing first-strand cDNA, the RNA was diluted (1 μg μL^{-1}). A cDNA kit (prime Script™) (TaKaRa BIO INC, Japan) was used following the manufactures instructions for cDNA synthesis and was stored at -80°C.

1.2.11 Quantitative real-time PCR (qPCR) analysis

The pro-inflammatory cytokine levels and the relevant protein expression levels were measured using the SYBR Green quantitative real-time PCR (qPCR). During the amplification process GAPDH was used as the internal reference standard. The process was completed using a Thermal Cycler Dice-Real Time System (TaKaRa, Japan). The primers used in the experiments were, GAPDH, iNOS, COX-2, IL-1β, IL-6, and TNF-α (sense and anti-sense). Primer sequences are provided in Table 1. 1.

The total mixture (10 μL) was comprised of diluted cDNA (3 μL); gene specific forward and reverse primers (each 0.4 μL of 10 pM); SYBR premix (5 μL); and ddH$_2$O (1.2 μL); 2× TaKaRa ExTaq™.

The thermal profile used for the analysis is as following: Stage 1: 95°C for 10 s; Stage 2: each 95°C for 5 s, 40 cycles; Stage 3: 55°C for 10 s; Stage 4: 72 °C for 20 s; Stage 5: 95°C for 15 s; Stage 6: 55°C for 30 s; and Stage 7: 95°C for 15 s. The method described by Livak and Schmittgen (2001) was used for the analysis of the relative expression levels [33].

1.2.12 Statistical analysis

Using a minimum of three samples, standard deviation was calculated in all experiments. The data is expressed as the mean ± standard deviation. A stat analysis program; IBM SPSS with one-way ANOVA was assisted in data analysis. $*p < 0.05$, $**p < 0.01$ vs. the PM treated group or $^\#p < 0.05$, $^{\#\#}p < 0.01$ vs. the un-stimulated group, were considered statistically significant.

Table 1. 1. Sequence of the primers used in this study.

Gene	Primer	Sequence
GAPDH	Sense	5′- AAGGGTCATCATCTCTGCCC-3′
	Antisense	5′-GTGATGGCATGGACTGTGGT-3′
iNOS	Sense	5′-ATGTCCGAAGCAAACATCAC-3′
	Antisense	5′-TAATGTCCAGGAAGTAGGTG-3′
COX2	Sense	5′-CAGCAAATCCTTGCTGTTCC-3′
	Antisense	5′-TGGGCAAAGAATGCAAACATC-3′
IL-1β	Sense	5′-CAGGATGAGGACATGAGCACC-3′
	Antisense	5′-CTCTGCAGACTCAAACTCCAC-3′
IL-6	Sense	5′-GTACTCCAGAAGACCAGAGG-3′
	Antisense	5′-TGCTGGTGACAACCACGGCC-3′
TNF-α	Sense	5′-TTGACCTCAGCGCTGAGTTG-3′
	Antisense	5′-CCTGTAGCCCACGTCGTAGC-3′

1.3. Results

1.3.1 Characterization of particulate matter

Certified reference material No. 28; China fine dust particulate matter (PM) was used for the experiments. Mori et al. (2008), reported the detailed procedure for collection of particulate matter through mechanical vibration and the chemical characterization [34]. We have referred the data provided by the National Institute for Environmental Studies, Ibaraki, Japan and supplied them below in the Figure 1.2 (b, c, d) for reference. Furthermore, a scanning electron microscope imaging was conducted in order to evaluate the particle size and distribution (Figure 1.2 a). It was evident that majority of particles possessing a diameter less than 5 µm.

(a)
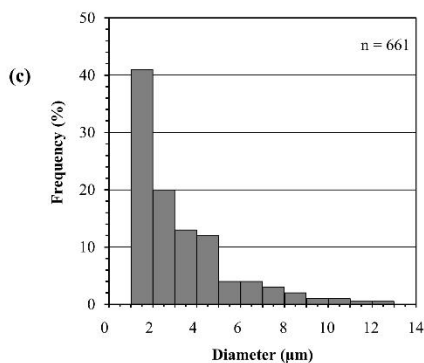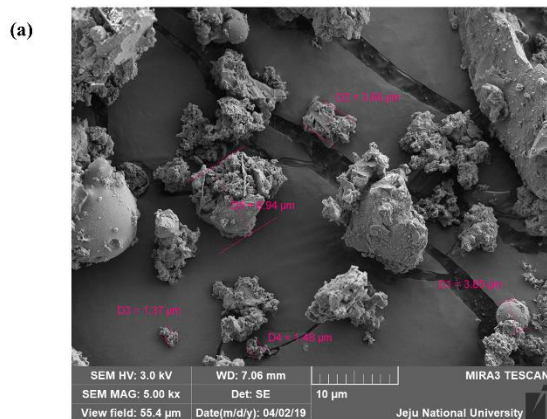
Element	Mass fraction (ppm)
Na	7960.0 ± 650.0
Mg	14000.0 ± 600.0
Al	50400.0 ± 1000.0
K	13700.0 ± 600.0
Ca	66900.0 ± 2400.0
Ti	2920.0 ± 330.0
Fe	29200.0 ± 1700.0
Zn	1140.0 ± 100.0
V	73.2 ± 7.0
Mn	686.0 ± 42.0
Ni	63.8 ± 3.4
Cu	104.0 ± 12.0
As	90.2 ± 10.7
Sr	469.0 ± 16.0
Cd	5.6 ± 0.4
Ba	874.0 ± 65.0
Pb	403.0 ± 32.0
U	4.3 ± 0.3

(b)

(c)

Element	Mass fraction (ppm)
Fluoranthene	7
Pyrene	4
Benz (a) anthracene	2
Benzo (b) anthracene	11
Benzo (k) anthracene	2
Benzo (a) pyrene	0.9
Benzo (a) perylene	2
Indeno (1,2,3-cd) pyrene	3

(d)

Figure 1. 2. Physical and chemical parameters of particulate matter (CRM No. 28) (a) Scanning electron microscopic (SEM) image. (b) Elemental composition as mass fractions. (c) Distribution of particle size. (d) Polycyclic aromatic hydrocarbon composition. Except the SEM image, figures were delivered from the NIES CRM No. 28 certificate.

15

1.3.2 Purification and structural characterization of fucosterol

The purification procedure was assisted by bioassay guided evaluation. Sample fractions potential to protect macrophages against PM stimulated inflammation and cytotoxicity was used for this. The chemical character was monitored via TLC. Stepwise details are provided in Figure 1.3, 1.4, 1.5. The pure compound expressed a white colour powdered texture. GC-MS analysis using a standard fucosterol purchased form Sigma-Aldrich revealed the yield of the isolated FST as 0.08% of the dry algal weight. Figure 1.6 depicts the GCMS analysis data for the purified compound. The molecular ion peak was observed at 412.40 and this agrees with the theoretical molecular weight of fucosterol (412.69 g mol^{-1}). Further, the fragmentation pattern and relevant fragments agrees with the library spectrum of NIST 11. The 1H and 13C data which are provided in the Figure 1.7, 1.8, 1.9 was used in the structure elucidation of FST. Moreover, HSQC and HMBC data were assisted to confirm the carbon multiplicity and carbon positons correlated to protons. Previously published data were referred in the structure elucidation [26, 28].
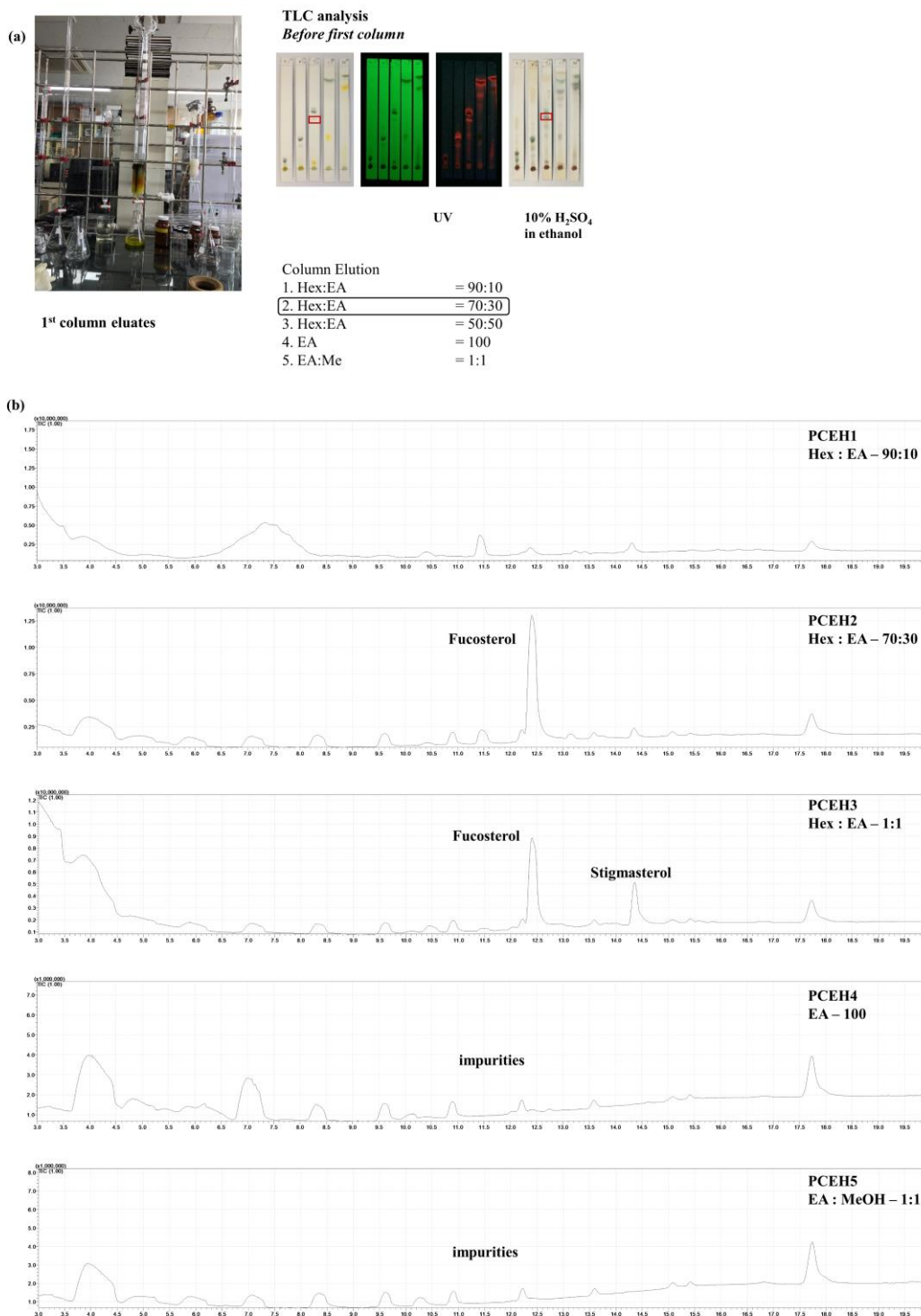
Figure 1. 3. Open column analysis chemical assay results. (a) First open silica column performance with TLC analysis. (b) GC-MS analysis data of each resulting fraction.
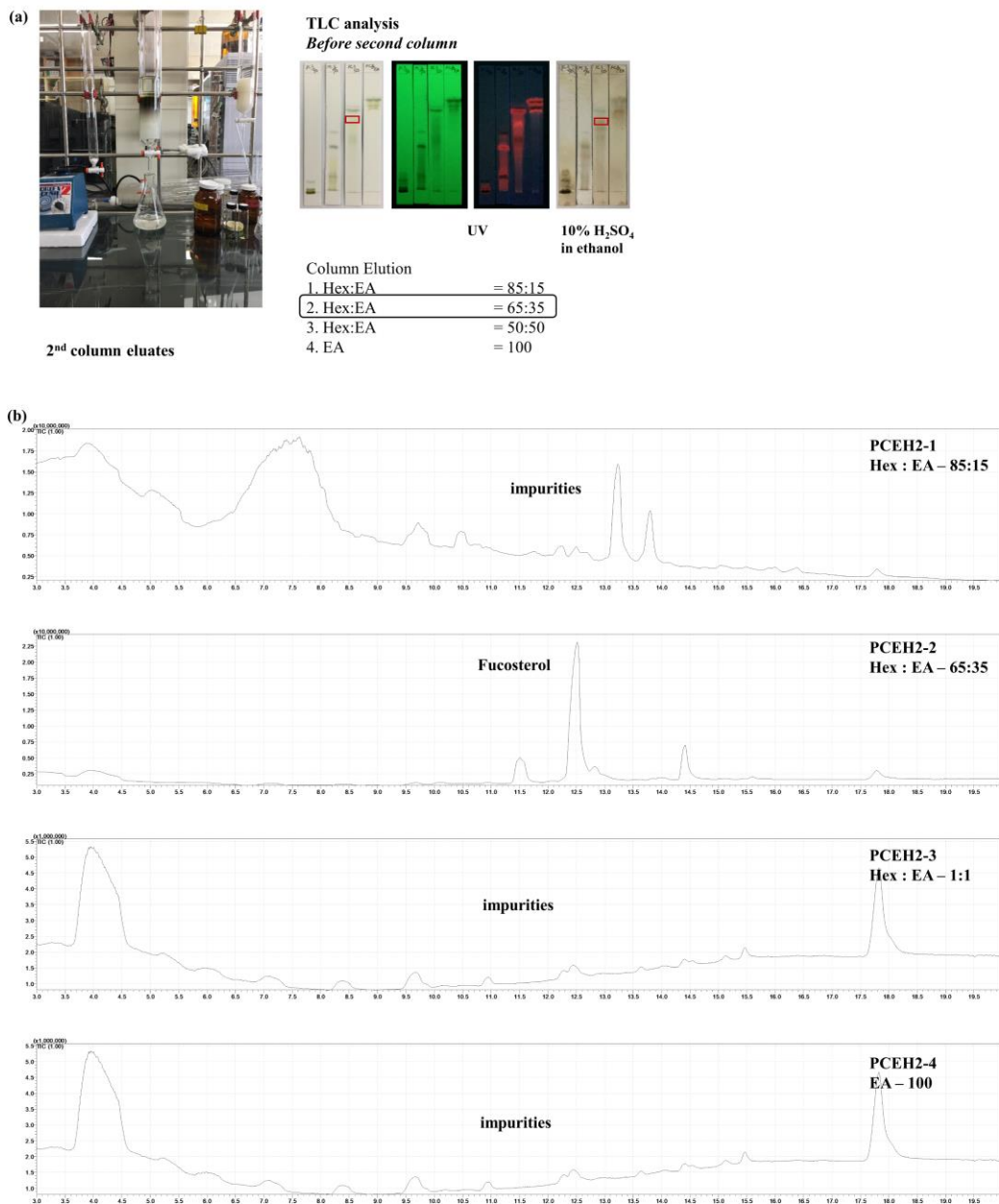
Figure 1. 4. (a) Second open silica column performance with TLC analysis (PCEH2). (b) Each resulting fraction GC-MS analysis.
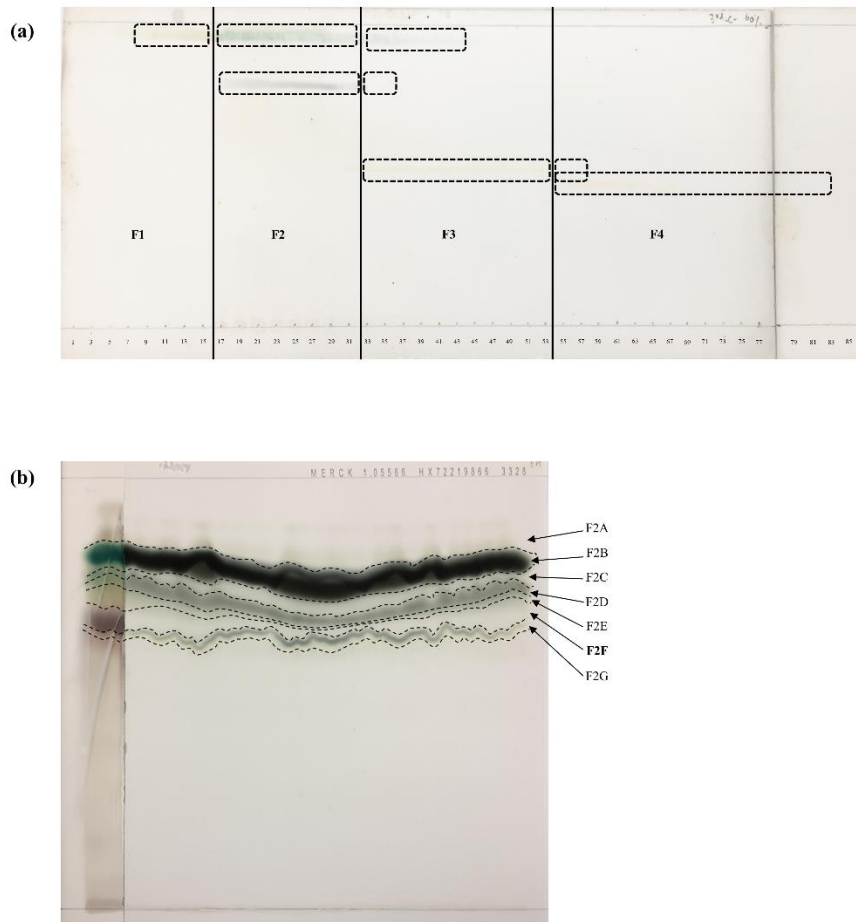
Figure 1. 5. (a) Purification of column fraction PCEH22 by a high resolution (lengthy) silica open column. (b) PTLC purification of PCEH22-F2.

Ion mass (m/z)	Fragment
412	$[M]^+$
397	$[M-CH_3]^+$
379	$[M-CH_3-H_2O]^+$
314	$[M-C_6H_{11}-CH_3]^+$
299	$[M-C_6H_{11}-2CH_3]^+$
281	$[M-C_6H_{11}-2CH_3-H_2O]^+$
229	$[M-\text{sidechain-ring D cleavage-}CH_3-2H]^+$
213	$[M-\text{sidechain-ring D cleavage-}CH_3-H_2O]^+$
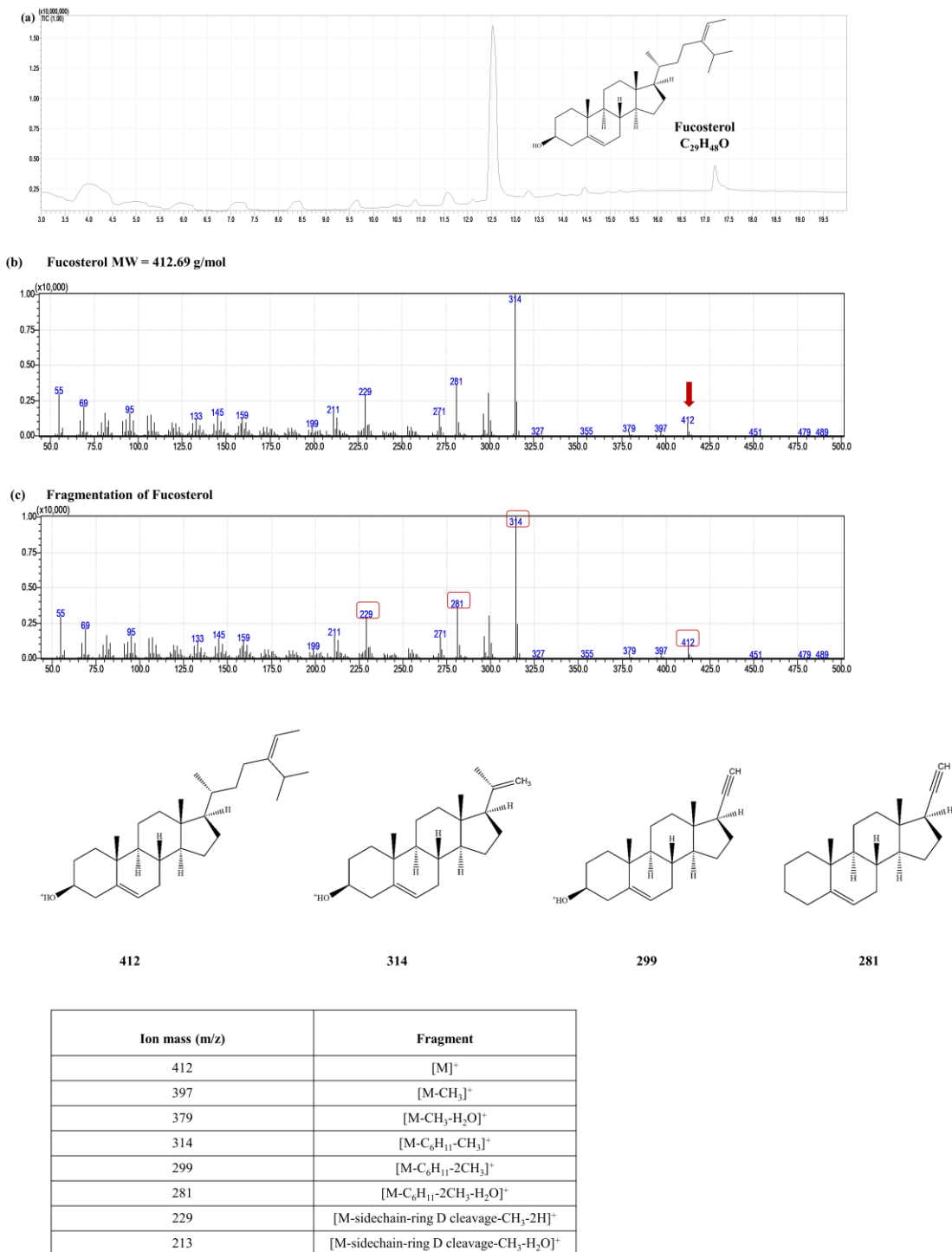
Figure 1. 6. (a) GC-MS/MS analysis of F2F. (b) The mass fragmentation pattern. (c) Predicted mass fragments of fucosterol corresponding to each prominent peak in the MS spectrum.
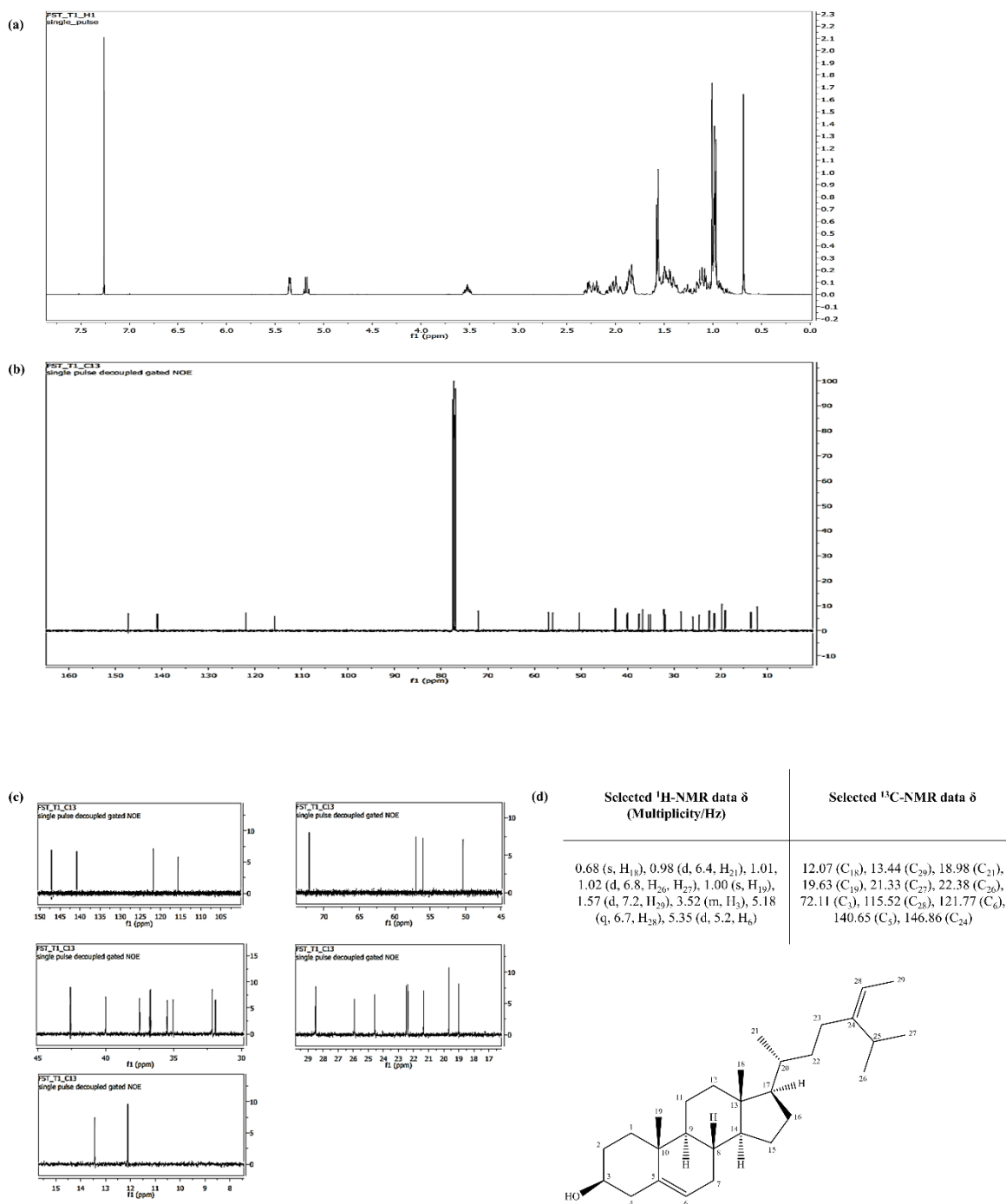
Figure 1. 7. NMR spectra of F2F in CDCl$_3$. (a) Proton NMR spectrum of F2F. (b) ^{13}C NMR spectrum of F2F. (c) Selected expanded regions in the ^{13}C NMR. (d) Selected NMR data tabulated with multiplicity.
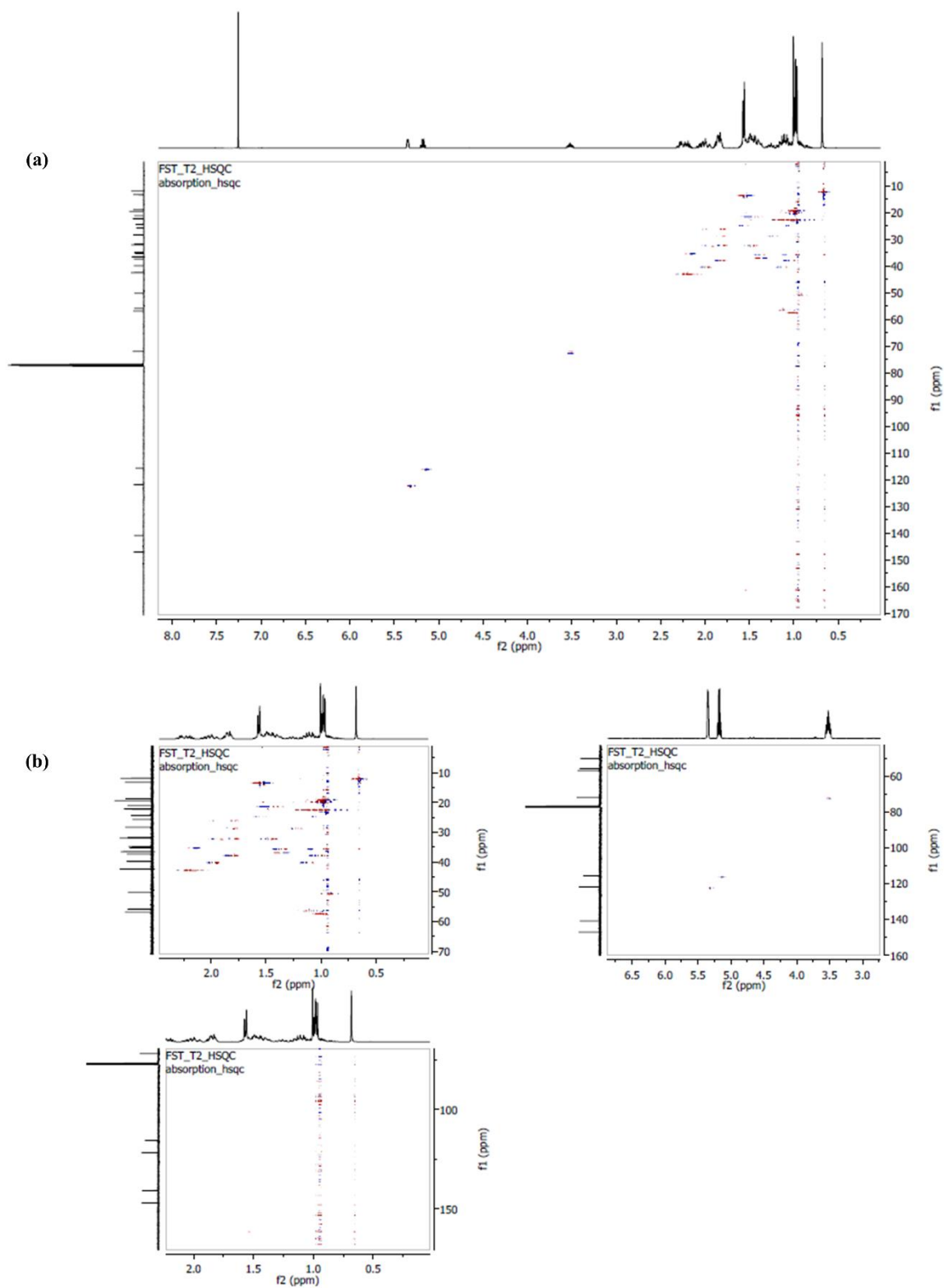
Figure 1. 8. 2D NMR spectra of F2F in CDCl$_3$. (a) HSQC spectrum of F2F. (b) Selected expanded regions of HSQC spectrum.

(c)

(d)
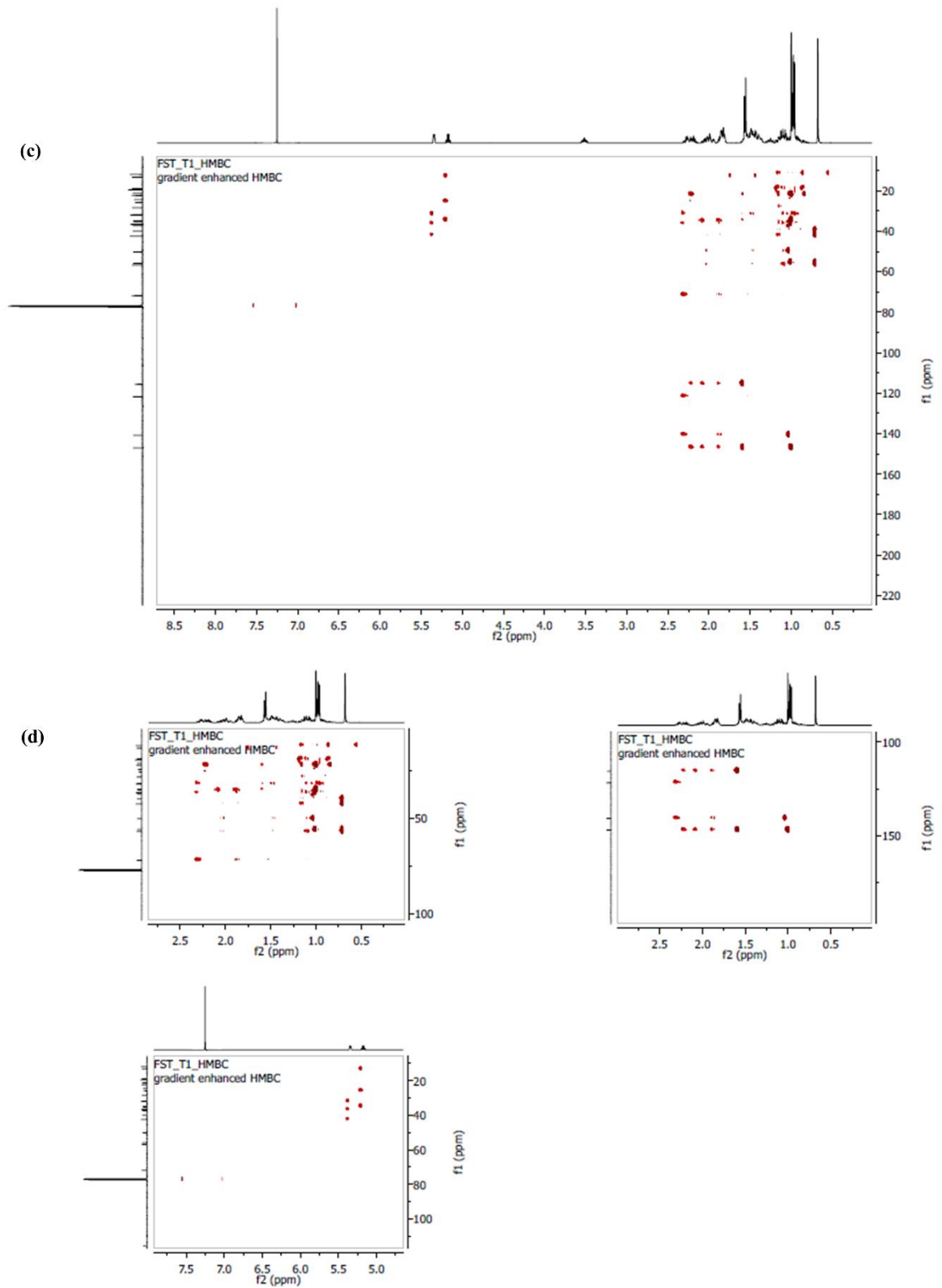
Figure 1. 9. (a) HMBC spectrum of F2F. (b) Particular magnified regions of HMBC

1.3.3 Effect of FST against PM induced cell viability and NO production

Figure 1. 10 (a, b) exhibits the behaviour of RAW macrophages against FST under PM stimulated conditions. NO production has been downregulated via the treatment of FST in a dose-dependent manner. The cell viability was significantly affected with the PM treatment but has recovered with the co-treatment of FST. LPS was used as a reference standard to compare the data of the PM stimulation. Accordingly, LPS affects the macrophages above the level of PM stimulation.
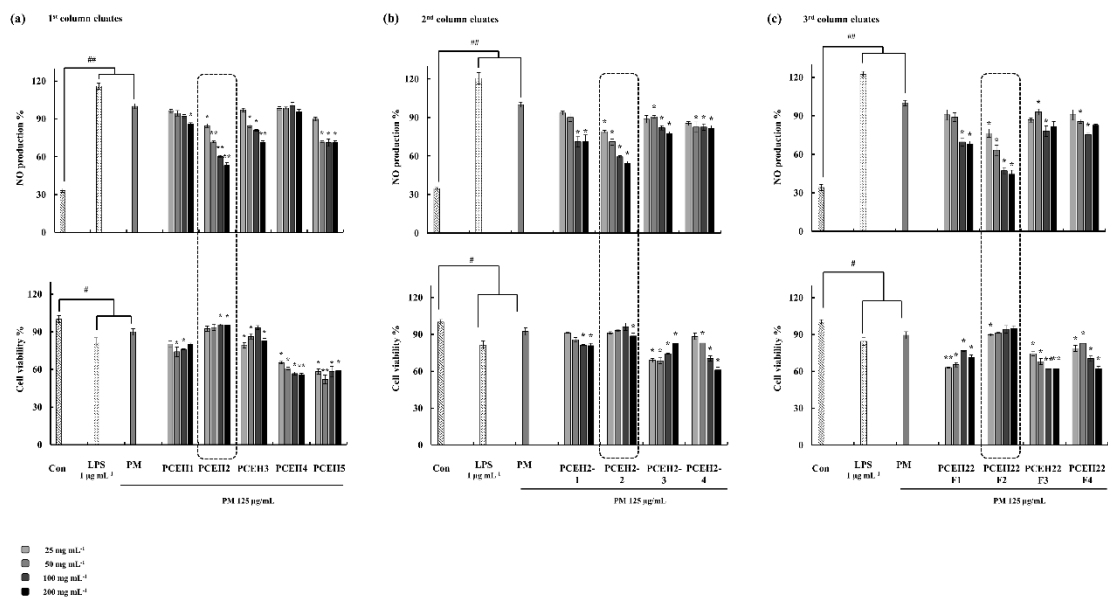
Figure 1. 10. Initial screening data for anti-inflammatory activity of each open column fraction against the particulate matter (CRM No. 28 – 125 µg mL^{-1}) induced conditions. (a) 1st open column fractions analysed for NO production and Cell viability. (b) 2nd open column fractions. (c) 3rd high resolution open column fractions. Triplicated experiments were used to evaluate the data and the mean value is expressed with ± SD. $*p < 0.05$, $**p < 0.01$ vs. the PM treated group or $^{#}p < 0.05$, $^{##}p < 0.01$ vs. the un-stimulated group.
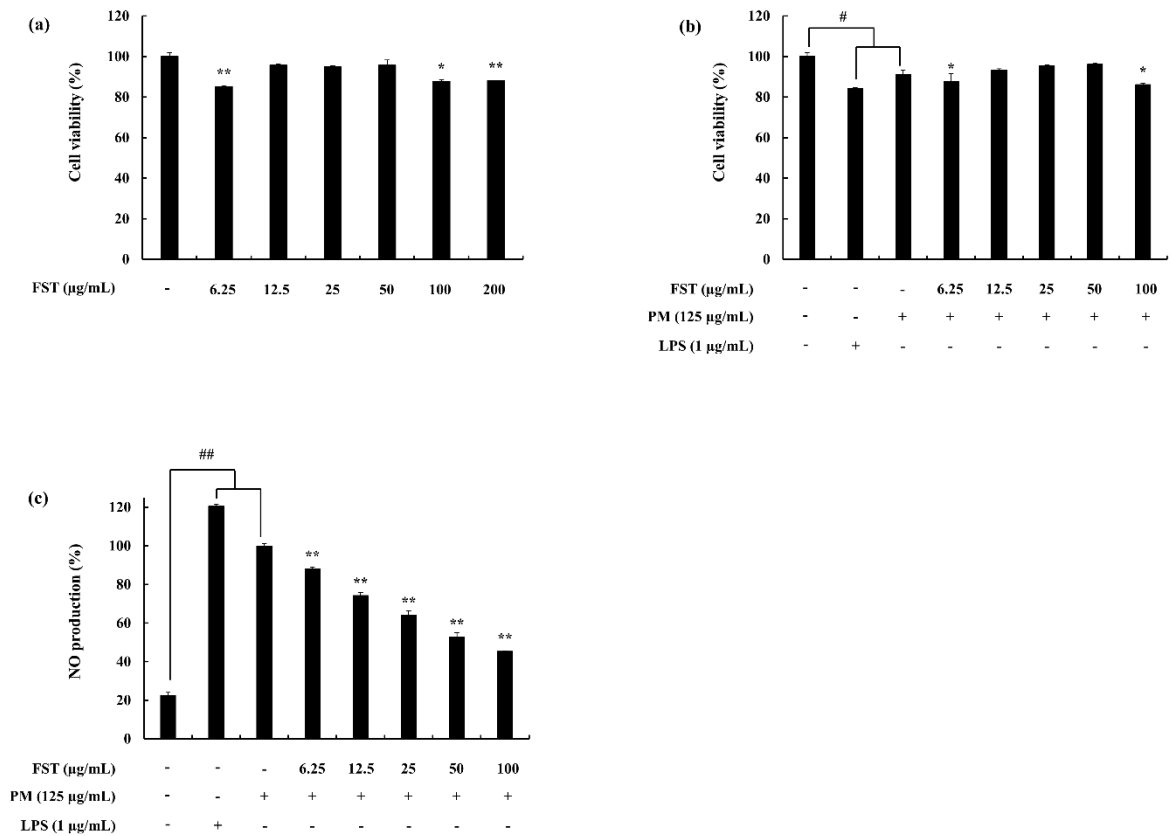
Figure 1. 11. (a) Cell viability evaluation against FST treated RAW 264.7 macrophages. (b) Cytoprotective and (c) NO inhibitory effect of FST, in PM-induced RAW 264.7. Cells were seeded, after 24h treated with FST (6.25 ~100 μg mL^{-1}), incubated for 1 h and co-treatment with culture medium or PM (125 μg mL^{-1}). Triplicated experiments were used to evaluate the data and the mean value is expressed with ± SD. $*p < 0.05$, $**p < 0.01$ vs. the PM treated group or $^{\#}p < 0.05$, $^{\#\#}p < 0.01$ vs. the un-stimulated group.

1.3.4 Pro-inflammatory cytokines and PGE₂ regulation in PM-induced macrophages assessed via ELISA, western blotting and gene expression

PGE_2 and cytokine analysis data (IL-1β, IL-6, and TNF-α) results (Figure 1.12) reveal that the levels which is increased due to the induction of PM has been significantly downregulated with the treatment of FST in a dose-dependent manner. The results are further supported via the gene expression analysis (Figure 1.13 a, b, and c). PGE_2 downstream is assisted by the downregulation of iNOS and COX-2 protein levels which are further confirmed via both the western blot and gene expression analysis (Figure 1.13 d, e, f, and g). The production of PGE_2 is mainly mediated through the COX-2.

The production of inflammatory mediators are also controlled via the mitogen-activated protein kinases (MAPKs) and nuclear factor κB (NF-κB) proteins. In the cytosol the p65 and p50 levels increase with the FST treatment while the respective phosphorylated levels are downregulated (Figure 1.13 a, b). This implies the ratio between phosphorylated forms to total form is down regulated dose dependently. A reciprocal pattern was observed in the cell nucleus where the total form of p50 and p65 downregulated with the sample treatment (Figure 1.14 c, d). MAPK pathway related proteins; the ratio between phosphorylated to total form has been down regulated similar to NF-κB cytosol expressions (Figure 1. 14 e, f). These results exhibit the PM-induced NF-κB nuclear translocation and MAPK phosphorylation has been inhibited by the activity of FST.
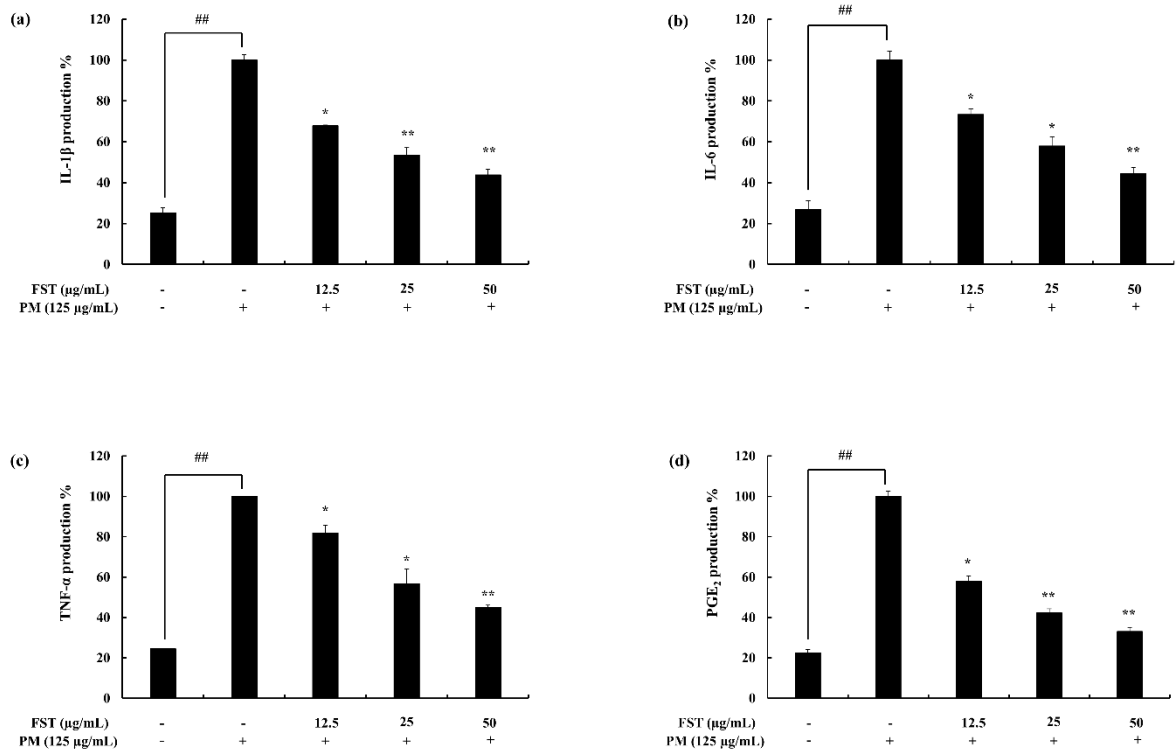
Figure 1. 12. Inhibitory effect of FST on the PGE_2 and pro-inflammatory cytokines (IL-1β, IL-6, and TNF-α) production in PM-induced RAW 264.7 cells conducted using ELISA. Culture supernatants of RAW 264.7 cells after successive treatment of PM, was used to quantify the inflammatory cytokines and PGE_2. Triplicated experiments were used to evaluate the data and the mean value is expressed with ± SD. $*p < 0.05$, $**p < 0.01$ vs. the PM treated group or $^{\#}p < 0.05$, $^{\#\#}p < 0.01$ vs. the un-stimulated group.
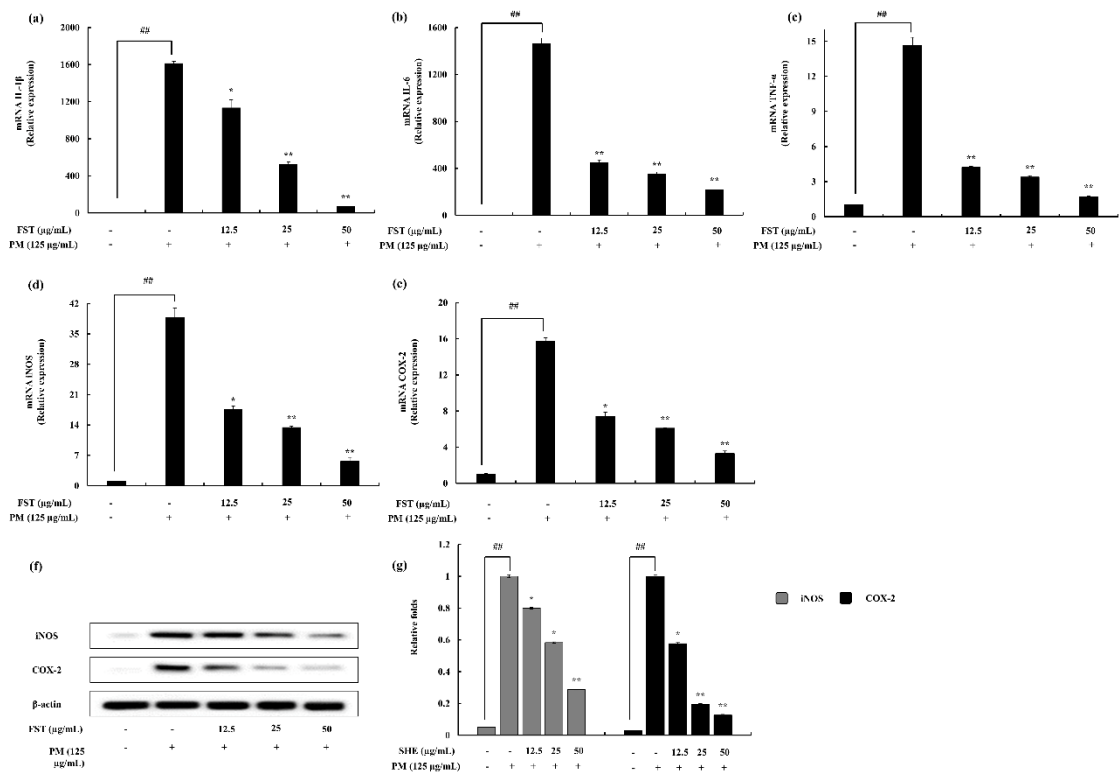
Figure 1. 13. Inflammation-associated gene expressions levels (a) IL-1β (b) IL-6 (c) TNF-α (d) iNOS and (e) COX-2. $2^{-\Delta\Delta Ct}$ method was used to calculate the relative mRNA levels. GAPDH used as an internal reference. Triplicated experiments and trials. mRNA significance relative to non-treated control was calculated using the Mann-Whitney U test. * = p < 0.05 and ** = p < 0.01. Inhibitory effects of FST on PM-induced inflammation associated protein in RAW264.7 cells. (f) iNOS and COX-2, determined using western blotting. (g) Quantitative data. β-actin (for cytoplasm) and nucleolin (for nucleus) were used as internal controls. Quantitative data was analysed using ImageJ software. Results are expressed as the mean ± SD of three separate experiments. *$p <$ 0.05, **$p <$ 0.01 vs. the PM treated group or [#]$p <$ 0.05, [##]$p <$ 0.01 vs. the un-stimulated group.
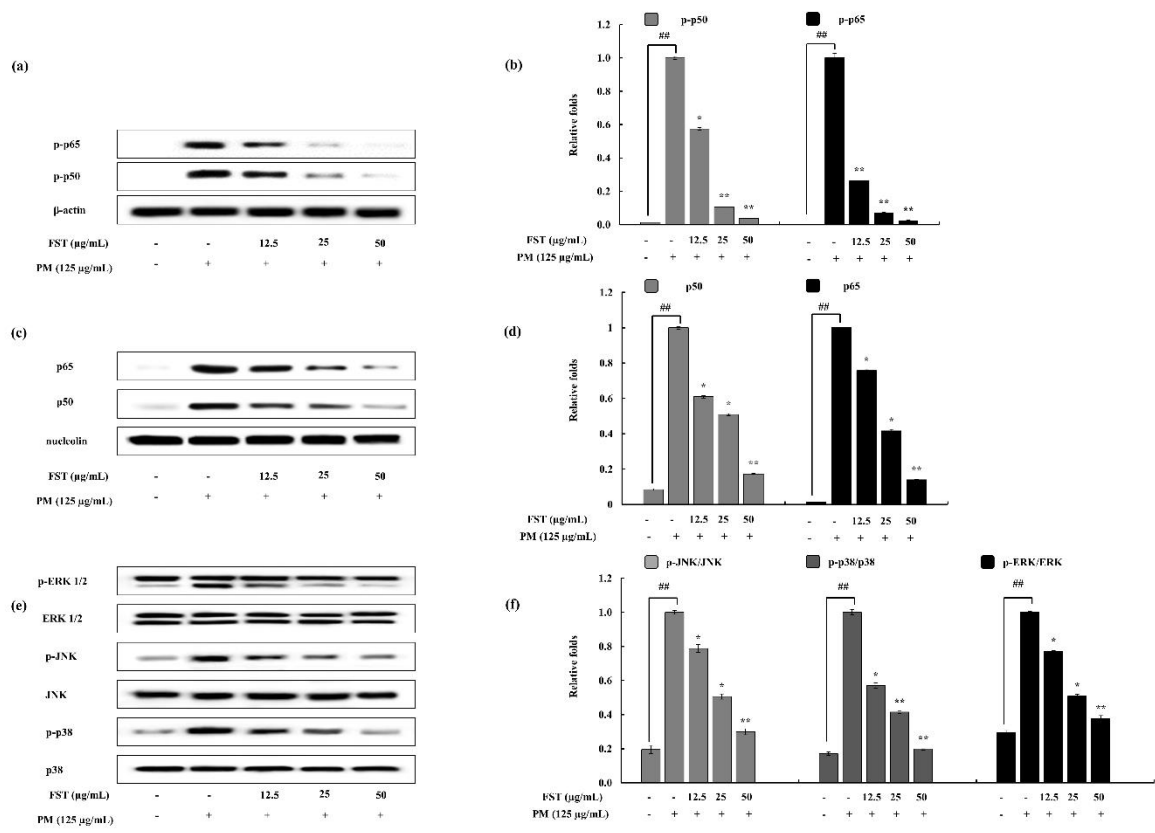
Figure 1. 14. Inhibitory effects of FST on PM-induced NF-κB and MAPK pathway associated protein in RAW 264.7 cells. (a) p50 and p65 in cytosol, (b) quantitative data, (c) p50 and p65 in nucleus (d) quantitative data, (e) p38, JNK and ERK, and relevant (f) quantitative data determined using western blotting. β-actin (for cytoplasm) and nucleolin (for nucleus) were used as internal controls. Quantitative data was analysed using ImageJ software. Results are expressed as the mean ± SD of three separate experiments. ∗$p < 0.05$, ∗∗$p < 0.01$ vs. the PM treated group or [#]$p < 0.05$, [##]$p < 0.01$ vs. the un-stimulated group.

1.3.5 Potential of FST on PM-induced macrophages in oxidative stress related pathway

Nrf2 and Keap1 in the cytosol observed to behave in opposing manner. The upregulated levels of Keap1 was downregulated with FST treatment while Nrf2 was upregulated (Figure 1.15 a, b). Nrf2 and HO-1 levels in the nucleus were upregulated with the co-treatment of FST (Figure 1.15 c, d). The results are supported via the activation of p38 MAPK pathway. p38 MAPK signals are mainly important in the regulation of Nrf2/ARE dependent upregulation of HO-1 levels in the purpose of reducing reactive oxygen species (ROS) amount in the cell [35]. The changing levels of Nrf2/HO-1 induce the production of cytoprotective factors against reactive oxygen species such as superoxide dismutase (SOD) and catalase.
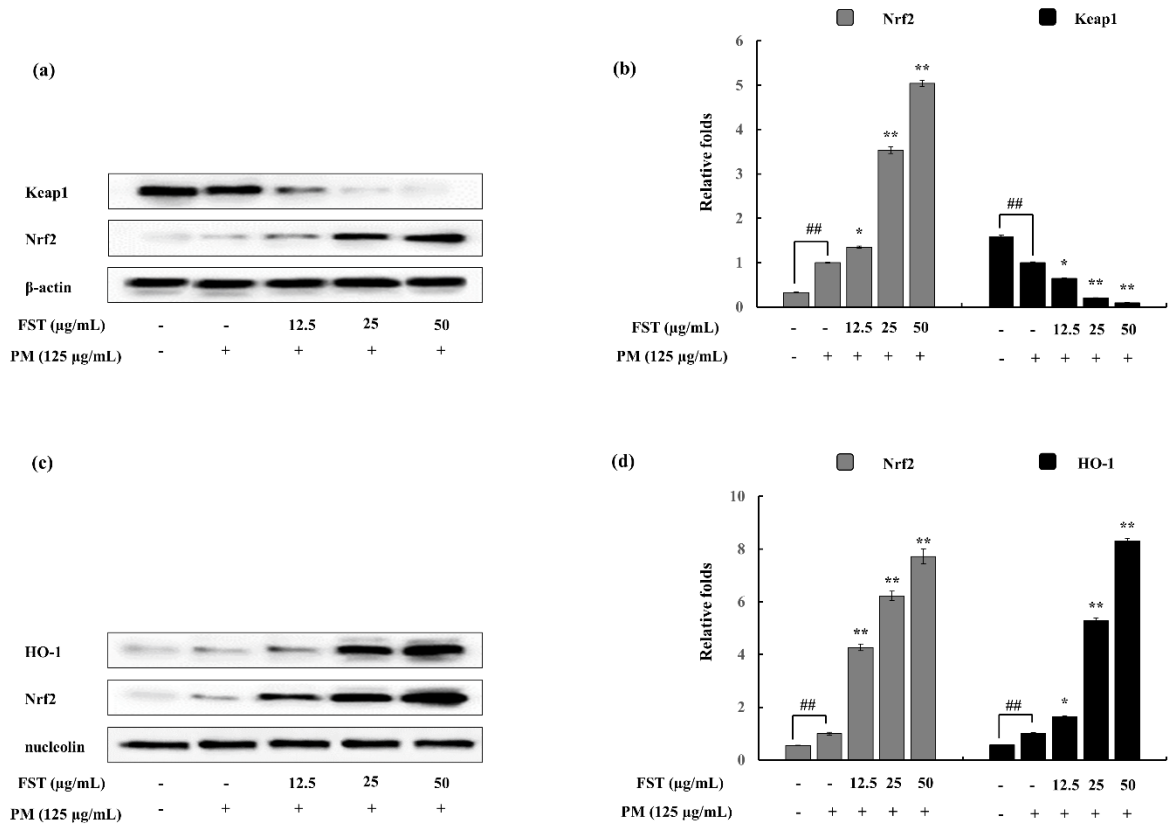
Figure 1. 15. Effects of FST on PM-induced oxidative stress associated protein in RAW 264.7 cells. (a) Nrf-2 and Keap1 in cytosol western blot, and (b) relevant quantitative data, (c) HO-1 and Nrf2 in nucleus western blot, and (d) relevant quantitative data. β-actin (for cytoplasm) and nucleolin (for nucleus) were used as internal controls. Quantitative data was analysed using ImageJ software. Results are expressed as the mean ± SD of three separate experiments. $*p < 0.05$, $**p < 0.01$ vs. the PM treated group or $^{\#}p < 0.05$, $^{\#\#}p < 0.01$ vs. the un-stimulated group.

1.4. Discussion

Air pollution can be addressed as the accumulation of diverse pollutants in the atmospheric phase of the globe which eventually causes harm to humans and other living organisms including natural environment [36, 37]. It's reported an estimated death toll above two million caused due to direct significances of air pollution throughout the globe annually. Further the damage is stated to be affected in the respiratory system [38]. The composition of PM is complex including both solid and liquid matter in varying sizes and chemical arrangement [39]. It was identified exposure to particulate matter causes numerous health issues such as respiratory symptoms, cardiovascular diseases, lung function disputes, and premature mortality [40, 41].

Brown algae are widely used in the East-Asia region as a food, nutraceutical and a pharmaceutical source. These include variety of biological properties including, anti-oxidant [42], anti-inflammatory [43], and antidiabetic properties [44]. This study selected a brown algae specie named *P. commersonii* which is abundant in the Laccadive sea, specifically from the shores of Fulhadhoo Island in the Maldives. *Padina* is a calcified brown algae and the thallus is flattened and fan-shaped. The distribution of the genus is marked in the temperate and tropical waters [45]. The research was focused on the hexane fraction of the ethanol extract of *P. commersonii*. Hexane fraction mainly contain sterols and lipids. In a majority of eukaryotic cells sterols are present as a significant family of lipids. Sterol synthesis follows different routes and due reason exhibit alterations among family classifications. Fucosterol is identified as a primary sterol in brown algae. Sanchez-Machado et al (2004), reports that in brown seaweed fucosterol is present above 80 % among sterols [46].

PM could easily penetrate through the respiratory tract. Human health is affected by these particles, in due course it could result in detrimental issues, including complications in respiratory tract and lead to allergic reactions and inflammation caused responses in macrophage cells. As human body consist of natural defence mechanisms, alveolar macrophages marks the first line of defence. Alveolar macrophages involve in phagocytosis of inhaled particles. As a model system during our study, the RAW 264.7 cell line was used. Against alien challenge and tissue injury, inflammation is a constructive host defence in order to restore the structure and function of the relevant systems. Both innate and adaptive immune responses are used depending on the situation by the human body [47]. Persisted inflammation could cause non-favourable conditions such as arthritis, multiple sclerosis and inflammatory bowel disease. Anti-inflammatory agents are used in the process and act via different mechanisms. Non-steroidal anti-inflammatory drugs (NSAIDs) are frequently used in treatments and they do not modify the pathogenesis of inflammation [48].

The results indicated a dose dependent down-regulation against PM induced inflammation. The cell viability which was significantly affected due to PM was successfully restored due to the treatment of FST. Inflammatory mediators such that PGE_2 was also inhibited by the potential of FST. ELISA evaluation of the pro-inflammatory cytokines such as IL-6, IL-1β, and TNF-α suggested the potent activity of FST. Similarly, iNOS and COX-2 were also observed to be down-regulated. Among these iNOS is important in the production of NO while PGE_2 production is influenced via the COX-2. iNOS is one of the many isoforms in the family of nitric oxide synthases (NOSs). Similarly, COX-2 is also a member of the COX family of enzymes and primarily regulate the production of PGE_2 against inflammatory conditions. [49, 50].

Cytokines can be defined as proteins involved in inter cellular communication. These are macromolecular proteins with higher molecular weights. Soluble cytokines are abundant while some can exist both in soluble and membrane bound forms [51]. The cytokine level measurement is conducted using numerous methods. Two major methods implied are cytokine immunoassays using protein levels (ELISA-enzyme linked immunosorbent assay) and mRNA levels by RT-qPCR. The antigen antibody specific affinity interaction is used in the immunoassays.

While macrophages are activated via inflammatory stimulants, the cells induce the production of inflammatory mediators such as nitric oxide (NO), prostaglandins and inflammatory cytokines, successively, leading to various signaling pathways [52, 53]. Though, the inflammatory mediators are helpful in down-regulating disorders, excessive production could cause detrimental effects. Inflammation is partially mediated via oxidative stress. Phull et al (2017), reports that ROS possesses dual roles. ROS induces mitogen responses at physiological concentrations while inclined levels cause damage the internal components of cells [54-56]. As a reflection of inflammation, the macrophages (neutrophils) overproduce ROS [57]. The pathogenesis of inflammatory disease could be provoked via the excessive inflammatory mediators which resulted from the ROS. It was reported that during chronic inflammation, ROS induces amplification of inflammatory signals via the NF-κB pathway related genes [58]. Therefore, the down-regulation or blockade of pro-inflammatory factors would emerge therapeutic approach for inflammatory disorders. The NF-κB pathway active molecules p50 and p65 reside in their inactive forms in the cytosol as IκB complex. Once the stimuli is passed, the free forms of p50 and p65 translocate to the nucleus leading the transcription of pro-inflammatory modulators [59]. The study results indicate under PM stimulated conditions FST, contribute up-regulation of the p50 and p65 total forms while phosphorylated forms

are down-regulated in the cytosol. Nuclear p50 and p65 levels are also up-regulated. The combined result suggests the potential of FST to inhibit PM-stimulated phosphorylation of the above complex, hence leading to anti-inflammatory effects.

Mitogen-activated protein kinases (MAPKs) are a family of serine/threonine protein kinases. Against external stimuli (stress signals) MAPK support to mediate basic biological processes via regulation of the synthesis of inflammatory mediators. This makes MAPKs as potential cross-points in inflammation therapeutics [60]. The activation of MAPK pathway lead to the activation of the transcription factor NF-κB [61]. Humans possess three distinct MAP kinase cascades; ERK1/2, JNK, and p38 MAP kinase. These are activated via different MAP kinase kinases (MKK). Among them MKK2 is responsible for the activation of ERK while JNK is triggered via MKK 4 and 7. p38 is activated through three MKKs namely, MKK 3, 4, and 6 [62, 63]. Cell growth, differentiation besides cell death and inflammation is associated with the p38 MAP kinase pathway [64]. Earlier studies report on the potential of fucosterol to inhibit the LPS-stimulated phosphorylation of p38 MAPK and MKK 3/6. Moreover several studies article on the influence of p38 MAPK with regard the activation of NF-κB [65, 66]. Hence, the results of our study can be correlated with the above as the p38 MAPK was down-regulated significantly due to FST treatment and NF-κB pathway evaluation signals (p50 and p65 phosphorylation) behaved in a similar manner. Despite the fact further studies regarding MKKs are required to solidify our result in between MAPK and NF-κB.

Nrf2/HO-1, which is an evolutionary conserved mechanism was used to briefly assess ROS involvement in the inflammatory diseases. Keap1 (Kelch-like ECH-associated protein 1) is an inhibitor protein, a cysteine-rich protein which is anchored to actin cytoskeleton. It is responsible for the cytosolic sequestration of Nrf2 under

physiological conditions. Keap1 promotes ubiquitination and degradation of Nrf2 under normal physiological conditions. Under stressful conditions which the Nrf2-dependent cellular mechanism is active (electrophiles and oxidants are rich in this stage), the Nrf2 is rapidly released from Keap1. Dissociated Nrf2 is translocated to the nucleus and binds to ARE. Keap1 also receives redox information or environmental cues via its highly reactive cysteine residues, and referred to as the sensor of the Nrf2-Keap1 system. The dissociation of the system is a relatively rapid event. The Nrf2 half-life time is approximately 20 min [67]. The breakdown of the system leads to Keap1 stabilization. Nrf2 also increase its half-life up to 200 min [68]. This allows successful nuclear translocation and cytoprotective gene transcription (HO-1) [69].

1.5. Conclusions

Fucosterol purified from *P. commersonii* exhibited effective potential against PM-induced inflammatory conditions in RAW 264.7 macrophages. NO, the distinct end product of inflammation was successfully inhibited via fucosterol under PM-stimulated conditions. Inflammatory mediators such as iNOS, COX-2, and PGE_2 as well as pro-inflammatory cytokines (IL-1β, IL-6, and TNF-α) were observed to be down-regulated dose-dependently with the treatment of FST. These results were further reinforced via the MAPK and NF-κB pathway signal molecule expression subdual. Nrf2/HO-1 pathway results suggested, ROS downregulation due to the activity of fucosterol. Thus, fucosterol could function as a potent protector against PM induced inflammatory diseases. In conclusion, the study provides an understanding of PM-stimulated cellular responses and mechanisms. Further in vivo studies would be beneficial to understand the detailed mechanisms and bioavailability of fucosterol on target organs.

Part II

Alginic acid from *Padina commersonii* abate PM-induced inflammatory responses

in keratinocytes and dermal fibroblasts

2.1. Introduction

Air pollution is supported via particulate matter (PM), and is comprised of heterogeneous mixture of components. These include volatile particles, organic matter, metals and ionic material [70]. The composition of the mixture varies depending on the source of generation. Both anthropogenic and natural sources contribute towards this phenomenon. The PM could cause health issues due to its accumulation in the atmosphere. Pulmonary toxicity as well as skin irritations are possible considering its constituents. Several studies have been conducted regarding PMs' effect on the respiratory system. Fernando et al (2017) reports on the influence of ERM-CZ100 (organic constituent fine dust) and ERM-CZ120 (inorganic constituents) on RAW macrophages and inflammation induction [71]. RAW macrophages were further assessed against CRM No.28, considering pulmonary issues and taking it as a model by Jayawardena et al (2018) [31].

When considering literature, it emphasizes two distinct sources of PM in the induction of inflammation. Several reports accounts the source to be the transition metal ion content which influences the inflammation via oxidative stress pathway. The oxidative stress arise due to the Fenton chemistry pathway implicated radicals are made responsible by some authors [72, 73]. The oxidative mechanism is most applicable to the smaller size PM, in which it possesses higher surface area and large number of particles. These have been evident to be higher in toxicity compared to its larger counterparts [74]. The second suggestion is the bacterial derived endotoxin bound to the surface of the particle cause of inflammation stimulation [10, 75].

The skin is the outermost barrier of the body and is susceptible to alien factors and these could cause inflammatory disorders. Due, reason anti-inflammatory agents applicable to skin are important. A distinct role of the skin is to provide immunity against

foreign matter and to become a critical point between the external and internal environments. Even though it can individually act as an immunological organ its effective function is observed with the resources supported from the immune system. A major component of the skin is its outermost keratinocyte layer. It performs immune function via the production of cytokines and responding to cytokines. The dermal component of the skin contains fibroblasts. This is traditionally not considered as a component of the immune system. But recent research suggests the crosstalk between the keratinocytes and the fibroblasts significantly contribute maintaining the homeostasis of the skin immune system [76]. These generate secondary cytokines such as IL-6. It was reported during wound healing the dermal fibroblasts contribute as a major source of keratinocyte growth factor (KGF) [77].

The present study conducted focusing on the effect of PM (CRM no. 28) on the skin cells. Selectively the keratinocytes and the inner layer fibroblasts; the extracted alginic acid from *P. commersonii* to inhibit the inflammation induced via PM. Marine algal polysaccharides have received much attention due to its high availability and ability for sustainable use as well as its biocompatibility. Alginate which is a polymer comprised mainly of β-D-mannuronic acid and α-L-guluronic acid forms hydrogels, chelate metals and performs anti-inflammatory, anti-oxidant properties [78, 79]. In this study, researchers believe the effect of transition metal ions causes the inflammation and the chelation ability of alginic acid reduces the subjective matter.

2.2. Methods

2.2.1 Materials

The certified reference material, CRM No. 28 (Urban aerosols), was purchased from the Centre for Environmental Measurement and Analysis, National Institute for Environmental studies, Ibaraki, Japan. The cell lines required for the experiments, HaCaT cells and the human dermal fibroblast (HDF) were purchased from the Korean Cell line Bank (KCLB, Seoul, Korea). Dulbecco's modified Eagle's medium (DMEM), fetal bovine serum (FBS), and antibiotics (penicillin and streptomycin) for growth medium were purchased from the GIBCO Inc. (Grand Island, NY, USA). 3-(4,5-dimethylthiazol-2-yl)-2,5-diphenyltetrazolium bromide (MTT) was obtained from Sigma-Aldrich (St. Louis, MO, USA). Antibodies used in the western blot analysis were from Santa Cruz Biotechnology (Santa Cruz, CA, USA). The cytokine kits used in the experiments were purchased from eBioscience (San Diego, CA, USA), R&D Systems (Minneapolis, MN, USA), BD Opteia (San Diego, CA, USA), and Invitrogen (Carlsbad, CA, USA). All the organic solvents used in the experiments were of analytical grade unless specified and were purchased form Sigma-Aldrich.

2.2.2 Alginic acid purification from *P. commersonii*

P. commersonii samples were collected from the coastal areas of Fulhadhoo Island, the Maldives. Samples were immediately washed with running water to remove salts and debris. The sample identification was assisted by Jeju Biodiversity Research Institute. Sample repositories were kept in the Laboratory of Marine Bioresource Technology at Jeju National University. Samples were then lyophilized and ground into fine powder. Alginic acid extraction followed the method described by Fernando et al. (2018) with some minor modifications [80]. An initial depigmentation was carried out,

42

first with hexane and was followed by 95% ethanol. This was then soaked in 10% formaldehyde (in ethanol) for 10 h, filtered and thoroughly washed with 95% ethanol in order to remove residual formaldehyde. The powder was air dried and lyophilized. This was immersed in distilled water and the pH was adjusted to 4.0 using diluted HCl. The pH of the suspension was maintained at 4.0 during the whole step. The mixture was agitated at 30 °C for 24 h, was filtered and washed with distilled water. The sample was then soaked in 5% Na_2CO_3 (w/v) and agitated at 30 °C for 24 h. The resulting extract was filtered and debris were clarified through centrifugation (10,000 × g, 4 °C for 10 min). The recovered supernatant pH was adjusted to 6.0 by addition of diluted HCl. This was treated with a saturated $CaCl_2$ solution and alginic acid was precipitated as calcium alginate. The pellet was recovered via centrifugation and suspended in 10% HCl for 2h (acid wash, 6×). Centrifugation was repeated to recover the pellet. Finally, the suspension was washed with distilled water and was neutralized using NaOH. The resulting alginate solution was extensively dialysed and lyophilized to obtain *P. commersonii* alginate powder (PCA).

2.2.3 Analysis of proximate composition of *P. commersonii*

The assessment included moisture, ash, protein, lipid and polysaccharide contents. Moisture by drying at 100 °C, ashing in a furnace at 600 °C for 5 h, protein content via kjedhal digestion, soxhelet method for lipids and polysaccharides by phenol sulphuric method. The Association of Official Analytical Chemists standard methods (AOAC 1990), were implemented in analysing the above of *P. commersonii*.

2.2.4 Evaluation of chemical composition of SHA

Chemical composition evaluation of an extract is an essential step before proceeding to further biological and physical properties. This includes assessment of polysaccharide, protein and polyphenol content.

The polysaccharide content was evaluated via the phenol sulfuric method as described by DuBois et al. (1956) [81], with minor modifications. Method in brief, a calibration standard curve was plotted using d-glucose 0 to 0.1 mg/ mL. Sample concentrations were maintained at 0.1 mg/ mL. Phenol (80%), 25 µL was treated into each tube. This was followed by the addition of 2.5 mL of conc. sulfuric acid and vortexed. The tubes were kept in dark at ambient temperature for 30 min. A volume of 200 µL from each tube was transferred to a 96 well plate and the absorbance was measured at 480nm.

The polyphenol content was measured accordingly with the method described by Chandler and Dodds [82], with minor modifications. Gallic acid was used as the standard and a calibration curve was plotted (0 to 0.1 mg/ mL). Samples were prepared to be 0.1 mg/ mL. Each test tube was introduced with 1 mL of 95% ethanol, was followed by 5 mL of distilled water and 0.5 mL of 50% (1N) Folin-Ciocalteau reagent. Tubes were vortexed and incubated for 1 h in dark environment. Subsequently, a volume of 200 µL was transferred to a 96 well plate and the absorbance was measured at 700 nm.

Protein percentages were quantified using Pierce™ BCA Protein Assay Kit and bovine serum albumin used as the standard.

2.2.5 Functional group analysis of PCA using FTIR

Powder method was used to analyze the functional groups via FTIR. Fourier-transform infrared spectroscopic (FTIR) analysis of the alginate was performed with a

Thermo Scientific NicoletTM 6700 FTIR spectrometer (Thermo Fisher Scientific, Waltham, MA USA). Potassium bromide (KBr) pellets were casted by combining 5 mg sample with 5 g KBr powder. A fine powder was generated using a mortar and pestle. KBr pellets were casted by applying pressure to the mould (5000-10000 psi). The pellets were then placed in the sample holder and scans (32) were collected within the range of 500-4000 cm^{-1} wavenumber having a resolution of 4 cm^{-1}. A background scan was collected initially. The results were analyzed using "Origin pro-2015" software package.

2.2.6 FTIR spectra interpretation using computational calculations

Gaussian view molecular modeling software was used to develop the Cartesian coordinates for the Gaussian calculations. Initial energy calculations; geometry optimization of the molecule was performed using B3LYP quantum mechanical methods. The molecule was optimized finely and the harmonic vibrational frequencies were performed by ab initio time-dependent density functional theory (DFT) calculations at B3LYP level using the 6-31G (d, p) basis set as described by Cardenas-Jiron et al. (2011) [83]. A scaling factor of 0.9645 was added to the calculated vibrational spectra.

2.2.7 Fine dust particle size estimation using SEM

The FD specimen was initially sputter coated with platinum. A Q150R rotary-pumped sputter coater (Quorum Technologies, Lewes, UK) was utilized for the purpose. The surface morphology of the CRM No. 28 particles were observed using a JSM-6700F field-emission scanning electron microscope (JEOL, Tokyo, Japan). The instrument was operated at 10.0 kV [31, 71] (Figure 1.2).

2.2.8 Maintenance of cell lines

HaCaT cell line was maintained in the DMEM medium which was supplemented with 10% FBS and 1% antibiotics. DMEM medium supplemented with F12 (25%), FBS (10%), and 1% antibiotics was used to maintain the human dermal fibroblast (HDF) cell line. The cells were maintained under controlled conditions as 5% CO_2 level and 37°C temperature. The cells were periodically subcultured and was used for experiments in its exponential growth phase.

2.2.9 Analysis of cell viability and intracellular ROS

The cytotoxicity was evaluated using the MTT assay in PM induced HaCaT and HDF cells. MTT colorimetric assay was performed in accordance with the method described by Mosmann et al. (1983) with slight modifications [29]. The cells were seeded with a concentration of 1×10^5 cells mL^{-1}, in 24 well plates. After a 24 h incubation period, PCA with different concentrations was treated. The growth media, DMEM was used to suspend the PM achieving a stock concentration. In order to obtain the treatment concentrations, a serial dilution was performed. PM was treated, given a 1 h incubation. Following a 24 h incubation period, MTT (2 mg/ mL in PBS) was added and incubated for another 3 h. Then the medium was aspirated and the formazan crystals were dissolved in DMSO. The absorbance reading was taken at 540 nm. The optimum PM treatment concentration was selected via this method.

The intracellular ROS levels were evaluated using the DCF-DA assay. The cells were seeded, samples were treated and following 1 h incubation period the cells were treated with DCF-DA reagent. This was incubated for 10 min and the fluorescence

intensity was determined at an excitation wavelength of 485 nm and emission wavelength of 535 nm [84].

2.2.10 PGE₂ and pro-inflammatory cytokine production level assessment

In order to obtain the cell culture media for the assessment of cytokine experiments, the cells were seeded in a similar manner described in the above experiments. HaCaT cells were seeded and incubated for 24 h. Samples were treated and after 1 h PM was treated. After 23 h incubation the media were retrieved for cytokine analysis. The culture media was collected separately and the expression levels of prostaglandin E2 (PGE_2), tumor necrosis factor α (TNF-α), interleukin (IL)-1β, and IL-6 were measured. The process was assisted with commercially available cytokine assessing kits and the test was performed in accordance with the given instructions by manufacturers.

2.2.11 Western blot analysis

To identify several key molecular mediators, western blot analysis was performed. The cells which were induced with PM were harvested within 30 min to analyze the upstream molecules in the MAPK and NF-κB pathway. Further 24 h incubation was continued to evaluate the COX-2 levels [80]. Ice-cold PBS was used to wash the harvested cells and was lysed using a Nuclear and cytoplasmic protein extraction kit (NE-PER®, Thermo Scientific, Rockford, USA). Each extract protein level was measured using BCA protein assay kit and was standardized (Bio-Rad, USA). Electrophoresis was carried out using sodium sulfate-polyacrylamide gels (12%). Subsequently, transferred onto nitrocellulose membranes. The membranes were blocked with skim milk and was incubated overnight with relevant primary antibodies; β-actin, COX-2, p38, p-p38, ERK1/2, p-

47

ERK1/2, JNK, p-JNK, p50, p-p50, p65, and p-p65 (Santa Cruz Biotechnology). Subsequent the incubation period, primary antibodies were removed and the HRP-conjugated secondary antibodies (anti-mouse IgG, Santa Cruz Biotechnology) were added. Then, signals were developed using the chemiluminescent substrate (Cyanagen Srl, Bologna, Italy). Membranes were photographed (FUSION SOLO Vilber Lourmat system) and the ImageJ program was assisted in the quantification of the band intensities [85, 86].

2.2.12 Spectroscopic analysis (ICP-OES)

Similarly, HaCaT cells were seeded and samples were treated. PM was treated following an incubation period. After the procedure the cells were harvested and collected into pre-weighted tubes. Cells were dried, and the final weight was taken. This was digested in concentrated HNO_3 using thermal energy (10% H_2O_2 was added). The acid digests were diluted in 3% HNO_3 acid. The metal ions were analyzed by inductively coupled plasma optical emission spectrometry (ICP-OES) system (PerkinElmer OPTIMA 7300DV, Inc., Waltham, MA, USA). The calibration curves were plotted using a multi element standard (PerkinElmer N9300233) including 10 ppm (10 µg/ mL) of each element (Mg, Al, K, Ca, Fe, Mn, Cu, Sr, Ba, Pb). The elements were detected by non-overlapping wavelengths ($\geq$2) [78]. Ultrapure deionized water was used in each step of the experiment. The final concentrations of the samples were calculated with reference to the calibration plots.

2.2.13 Statistical analysis

Based on triplicated experiments, data are expressed as means ± SD. One-way ANOVA and Duncan's multiple range test was used to determine the significant

differences among data values. $*p < 0.05$, $**p < 0.01$ vs. the PM treated group or $^{#}p <$ 0.05, $^{##}p < 0.01$ vs. the un-stimulated group, were considered statistically significant. SPSS v. 20 (IBM Corp., Armonk, NY, USA) was used to perform all the statistical analyses.

2.3. Results

2.3.1 Proximate composition and chemical composition

The proximate composition results provides a better understanding of the nutritional components of the selected seaweed. The results are tabulated in Table 2.1. Accordingly, *P commersonii* is consisted of higher amount of crude polysaccharides (57.87 ± 0.63). Crude proteins are also present in the sample (16.36 ± 0.32). The ash content was reported as 14.14 ± 0.72, symbolizing higher mineral content due to its natural habitat. The moisture content was 6.2 ± 0.54, while the lipid content was reported as the lowest (1.03 ± 0.25). Table 2.2 indicates the chemical composition of the purified alginate (PCA).

Table 2. 1. Proximate chemical composition of *P. commersonii*

Composition	Content (%)
Moisture	6.2 ± 0.54
Ash	14.14 ± 0.72
Protein	16.36 ± 0.32
Lipid	1.03 ± 0.25
Polysaccharide	57.87 ± 0.63

Table 2. 2. Chemical composition of purified alginic acid from *P. commersonii*

Composition	Content (%)
Polysaccharide	79.84 ± 1.32
Ash	3.42 ± 0.56
Protein	1.22 ± 0.18
Polyphenol	2.17 ± 0.69
Yield	16.85 ± 0.32

Results represent mean ± standard deviation of at least triplicate determinations

2.3.2 Structural characterization of PCA

The structure of the PCA was characterized by FTIR analysis (Figure 2.1). Distinct peak patterns were referred with the commercial sodium alginate available. The prominent peaks were also referred with the early reports published. It was confirmed that PCA well aligns with the commercial level alginic acid. O-H stretching vibrations were observed in the range of 3425 cm^{-1}. Carboxylic group stretching vibrations were visible in 1680 cm^{-1} and 1420 cm^{-1} [87]. Further these data were referred with the pre-defined spectral features obtained via computational quantum chemistry calculations. The constructed disaccharides were analyzed via Gaussian software to generate Cartesian coordinates. These were optimized using semi-empirical methods. This was subjected to the harmonic vibrational calculations with time dependent density functional quantum chemical (DFT) theory using B3LYP level, 6-31G (d,p) basis set. Figure 2.2 indicate the resulting structure geometry of dimers constructed, their free energies calculated and the vibrational spectroscopy obtained.
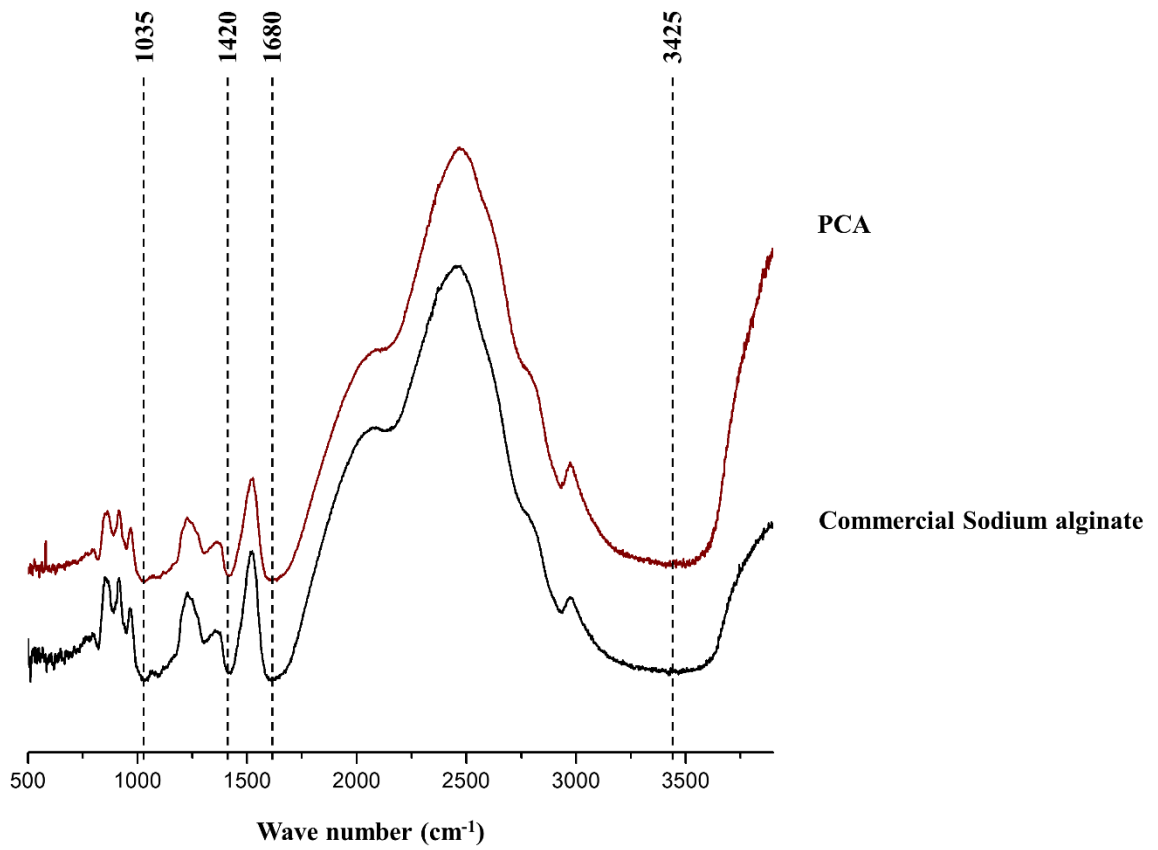
Figure 2. 1. FTIR spectroscopic analysis of PCA compared with commercial sodium alginate

(a)

Molecular mass: 370.07474 amu.
Zero-point vibrational energy 958.3359 (kJ/mol)
Free energy = -1437.709634 Hartree/particle
Free energy = -3774706.931609 kJ/mol

(b)

β-D-mannuronic acid   α-L-guluronic acid
C1 and C4 equatorial groups C1 and C4 axial groups

(c)

Wavenumber (cm⁻¹)
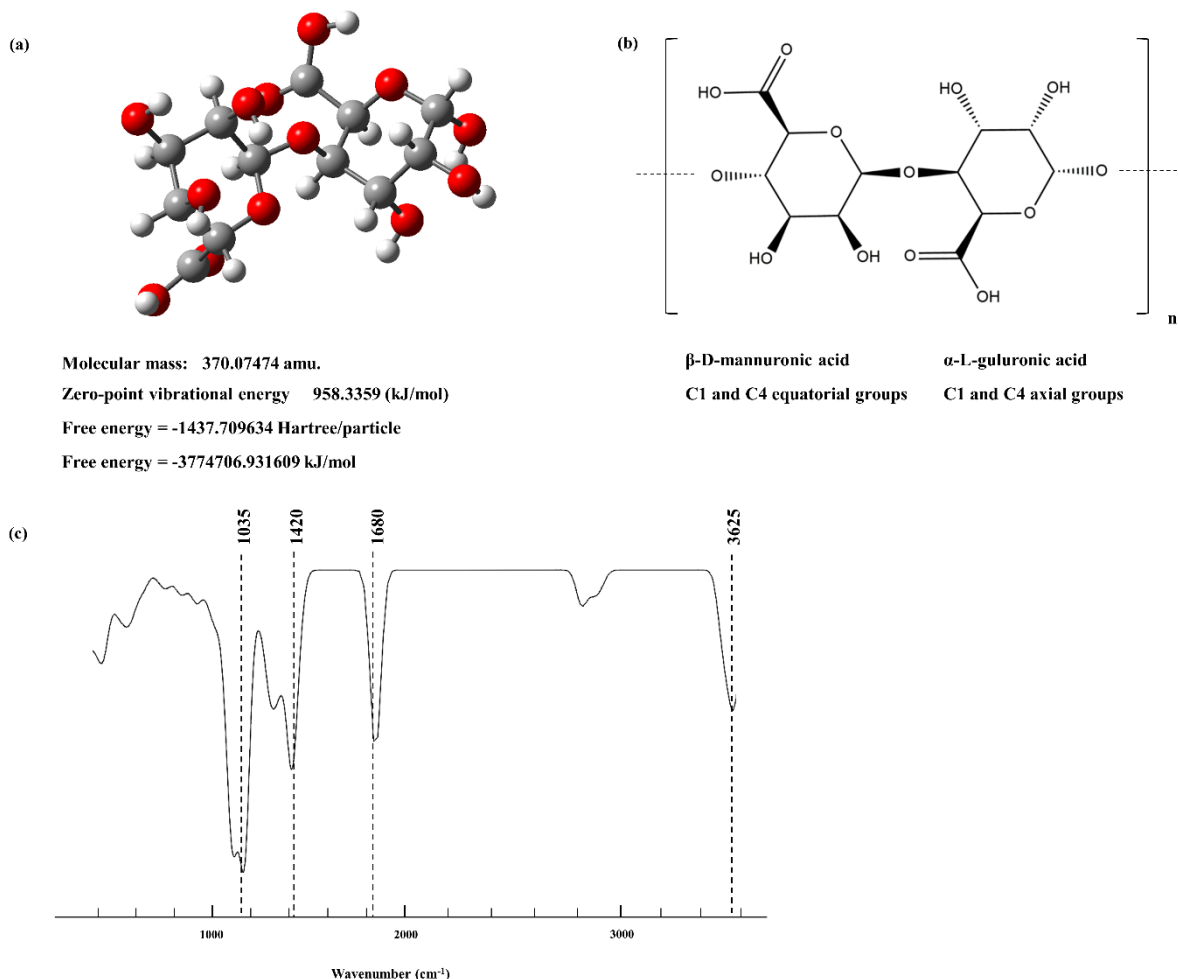
Figure 2. 2. Characterization of alginic acid with computational calculations using Gaussian software. (a) Structure of constructed dimeric unit of alginic acid 3D and standard free energy. (b) Skeletal formula of alginic acid dimer with its individual monomeric units representing stereochemistry in 2D. (c) Vibrational spectra of alginic acid dimer calculated and constructed with density functional quantum chemical (DFT) calculations using B3LYP level, 6-31G (d,p) basis set

2.3.3 Potential of PCA to reduce PM-stimulated inflammatory responses in keratinocytes and fibroblasts

The treatment of PCA resulted in recovery of the cell viability which was downregulated due to the stimulation of PM in keratinocytes (Figure 2.3, 2.4). Similarly, the ROS level was dose-dependently downregulated. NO levels or iNOS production was not evident during the study. A significant upregulation of the pro-inflammatory mediators including PGE_2 and its modulator COX-2 was observed with the treatment against PM. This was successfully downregulated via the treatment of PCA. Similar trend was evident with the pro-inflammatory cytokines; IL-1β and IL-6. However, in our experiments the level of TNF-α expression was altered in negligible amounts (Figure 2.5).
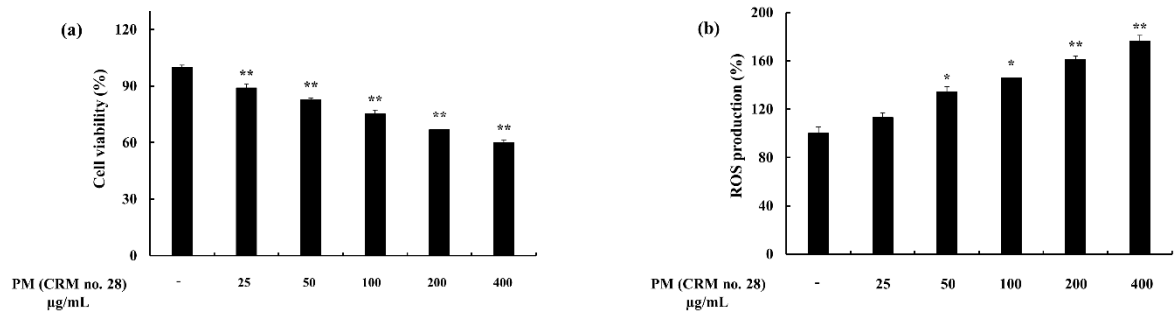
Figure 2. 3. Particulate matter induced keratinocytes. (a) Cell viability measured via MTT assay. (b) ROS production measured via DCF-DA assay. Triplicated experiments were used to evaluate the data and the mean value is expressed with ± SD. $*p < 0.05$, $**p < 0.01$ vs. the PM treated group or $^{#}p < 0.05$, $^{##}p < 0.01$ vs. the un-stimulated group.
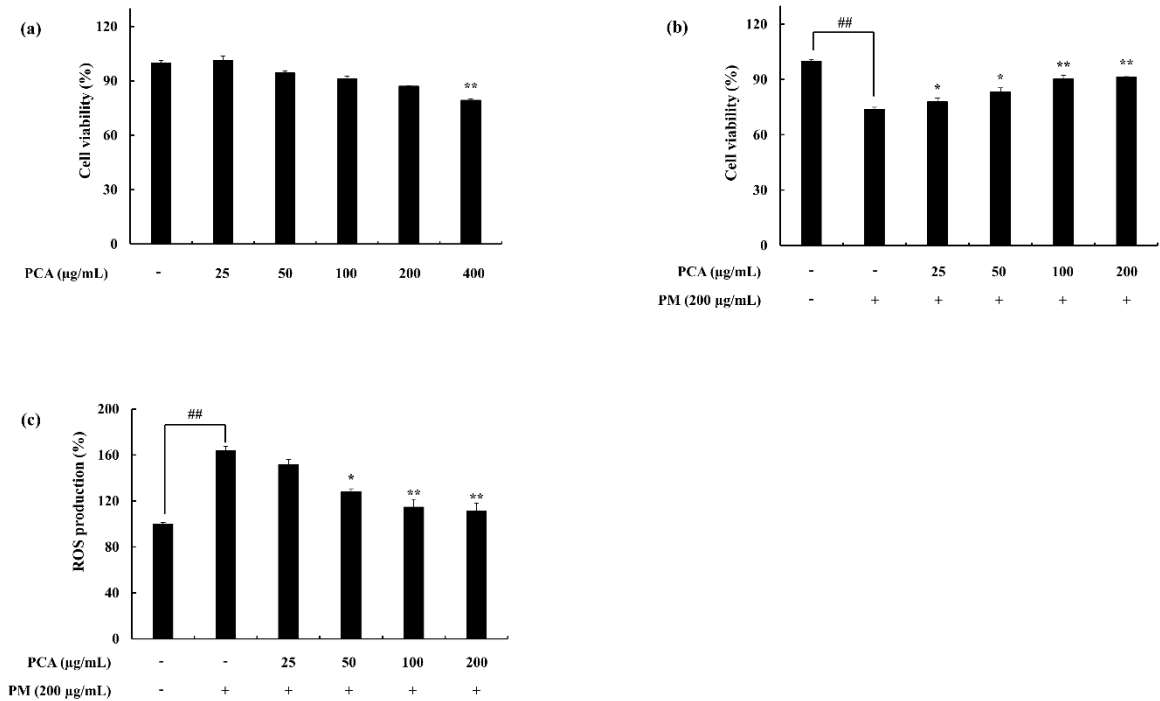
Figure 2. 4. (a) Cell viability evaluation against PCA treated keratinocytes. (b) Cytoprotective and (c) ROS production inhibition effect of PCA, in PM-induced keratinocytes. Cells were seeded, after 24h treated with PCA ($25 \sim 200$ μg mL^{-1}), incubated for 1 h and co-treatment with culture medium or PM (200 μg mL^{-1}). Triplicated experiments were used to evaluate the data and the mean value is expressed with ± SD. $*p < 0.05$, $**p < 0.01$ vs. the PM treated group or $^{\#}p < 0.05$, $^{\#\#}p < 0.01$ vs. the un-stimulated group.
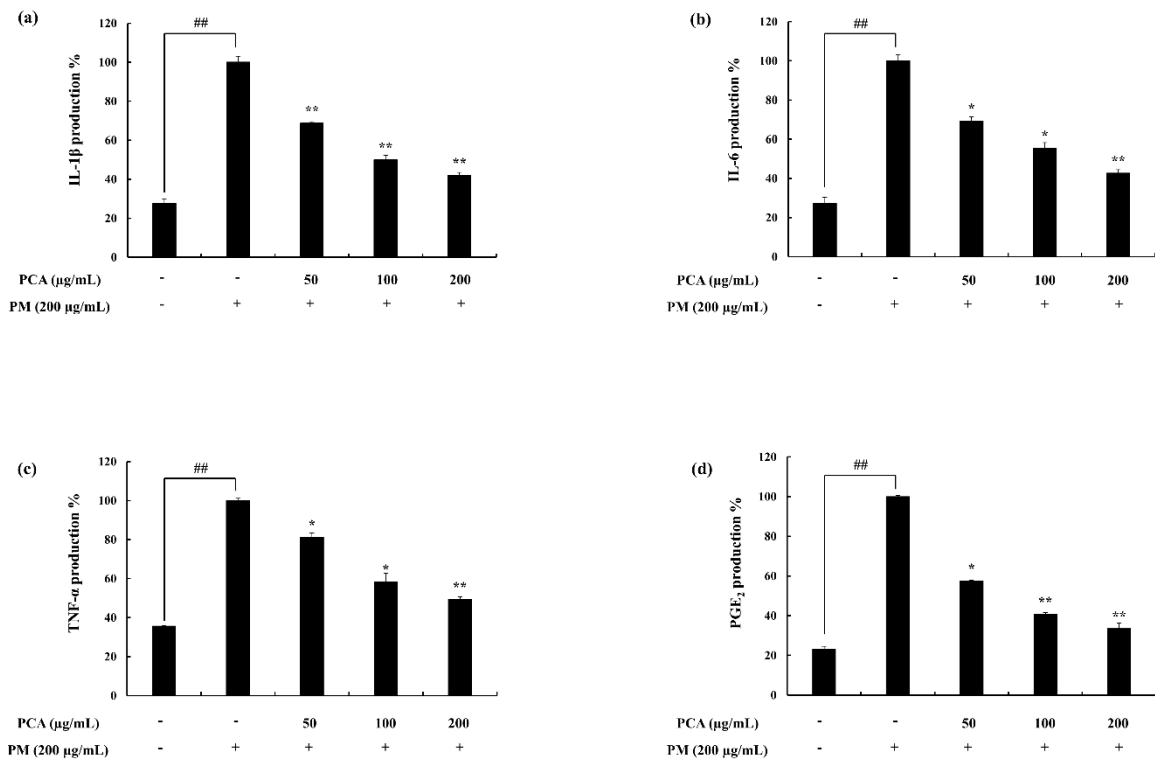
Figure 2. 5. Effect of PCA on the keratinocytes and its production of inflammatory mediators (PGE$_2$) including cytokines (IL-1β, IL-6, and TNF-α). Culture supernatants were collected after successive treatment of PM and used to quantification using ELISA. Triplicated experiments were used to evaluate the data and the mean value is expressed with ± SD. t-test was used to calculate the level of significance. $*p < 0.05$, $**p < 0.01$ vs. the PM treated group or $^{\#}p < 0.05$, $^{\#\#}p < 0.01$ vs. the un-stimulated group.
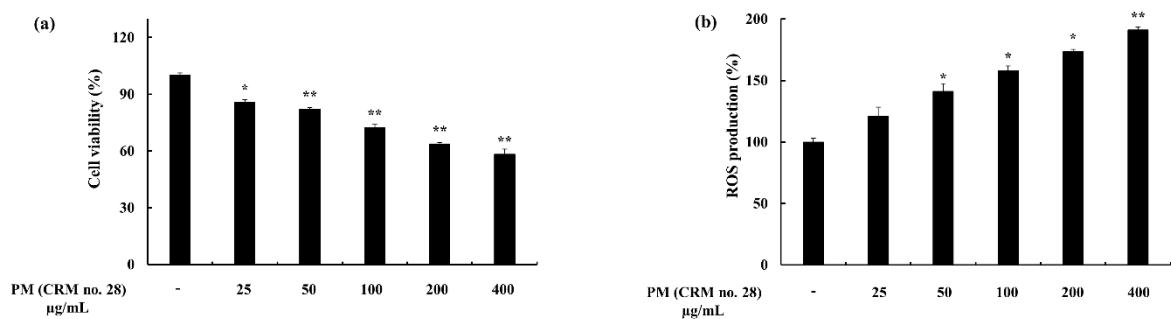
Figure 2. 6. HDF cells induced via particulate matter. (a) Cell viability against PM induction. (b) ROS production assessed by DCF-DA assay. Triplicated experiments were used to evaluate the data and the mean value is expressed with ± SD. $*p < 0.05$, $**p < 0.01$ vs. the PM treated group or $^{\#}p < 0.05$, $^{\#\#}p < 0.01$ vs. the un-stimulated group.
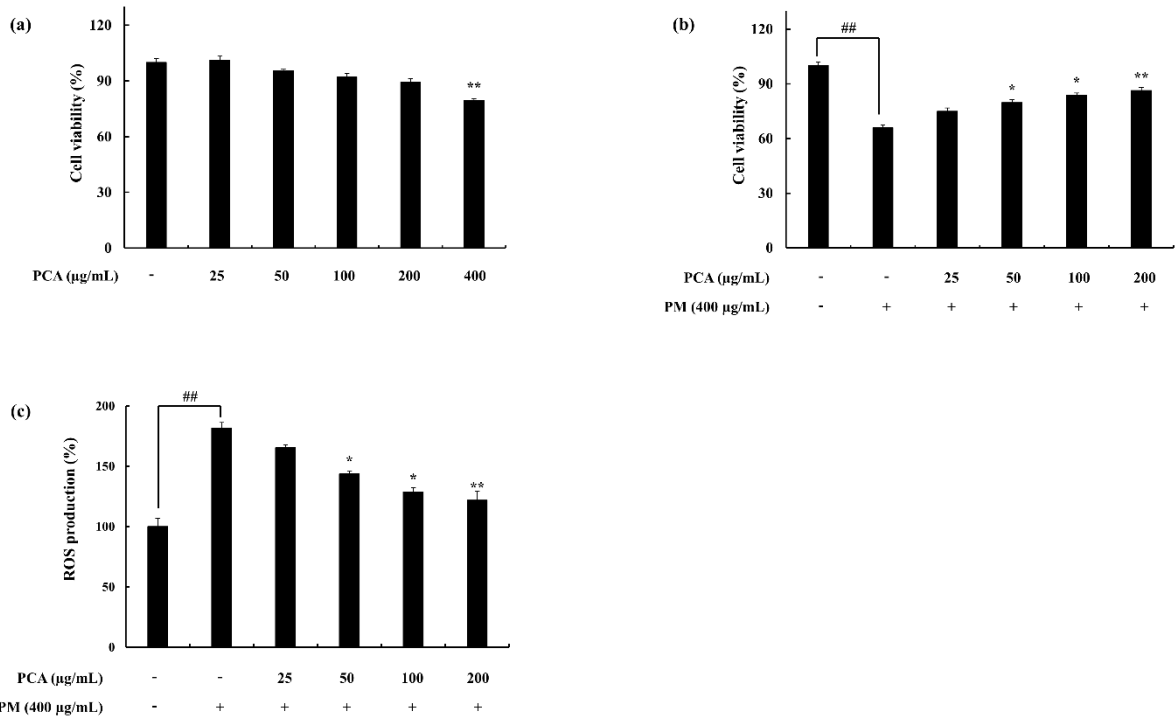
Figure 2. 7. (a) HDF cells treated with PCA and evaluated cell viability. (b) Cytoprotective and (c) ROS production inhibition effect of PCA, in PM-induced HDF. Cells were seeded, after 24h treated with PCA (25 ~200 μg mL^{-1}), incubated for 1 h and co-treatment with culture medium or PM (400 μg mL^{-1}). Triplicated experiments were used to evaluate the data and the mean value is expressed with ± SD. $*p < 0.05$, $**p < 0.01$ vs. the PM treated group or $^{#}p < 0.05$, $^{##}p < 0.01$ vs. the un-stimulated group.

2.3.4 Potential of PCA to abate PM induced inflammatory responses via NF-κB and MAPK pathways

In the process of evaluating the activity of PCA as an anti-inflammatory agent, this research subsequently assessed whether or not the inhibition of inflammation responses are mediated via the NF-κB and MAPK pathways. The PM induced phosphorylation of p38, ERK1/2, and JNK MAPKs in keratinocytes were considered via western blotting. As illustrated in the Figure 2.8 (c, d), PM encouraged the phosphorylation of MAPK mediators. PCA treatment (50, 100, and 200 µg mL^{-1}) gradually down regulated the phosphorylation process of p38, ERK1/2, and JNK. Among the MAPKs p38 exhibit significant down regulation while ERK1/2 remains as the least affected of all three. Cytosolic p-50 and p-65 mediators were observed to be phosphorylated against PM induction and was successfully downregulated via the PCA treatment. Figure 2.8 (a, b) indicates the ratio between phosphorylated to total form variation of NF-κB related signals. Results applicable to HDF cells are represented in the Figure 2.9.
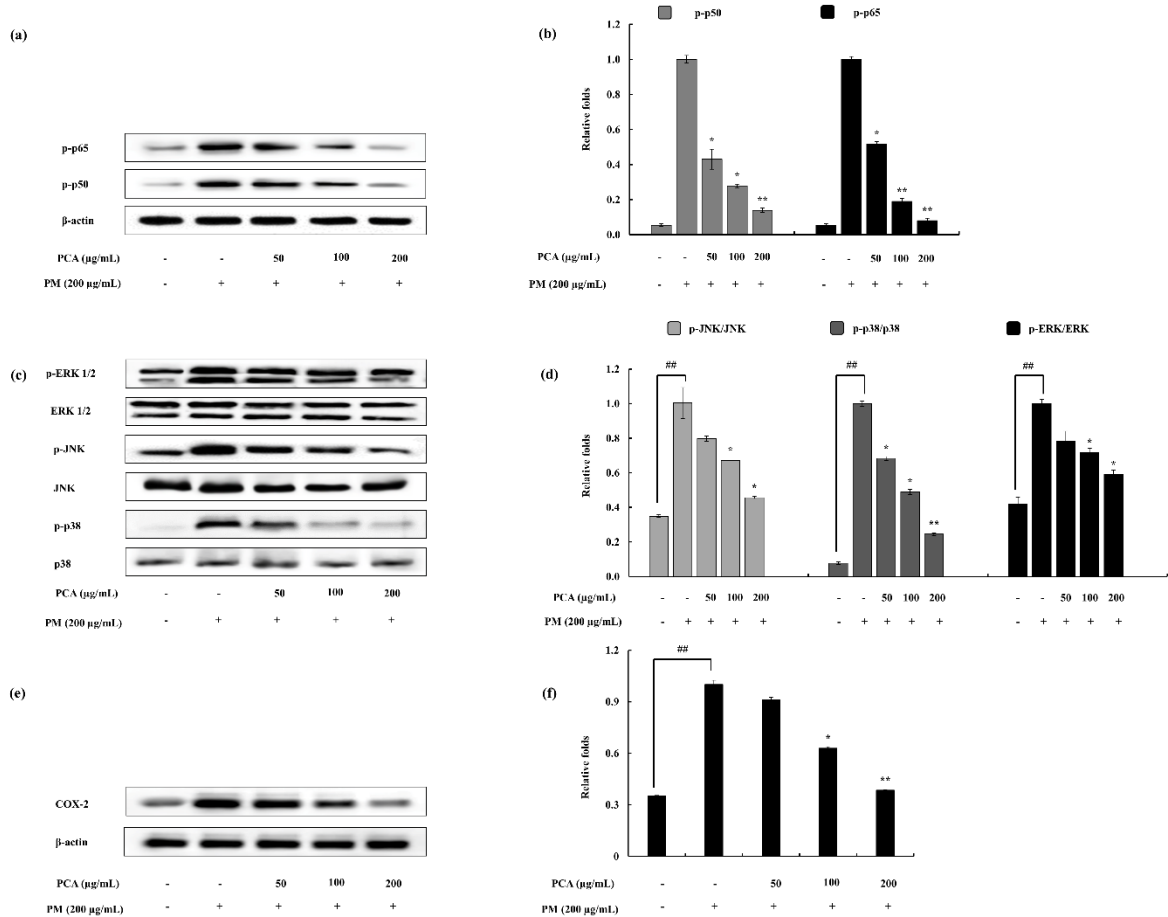
Figure 2. 8. Effect of PCA on keratinocytes to inhibit NF-κB associated signals, MAPK pathway molecules and COX-2. (a) p50 and p65 in cytosol, (b) quantitative data, (c) p38, JNK and ERK, (d) quantitative data, (e) COX-2 and relevant (f) quantitative data determined using western blotting. β-actin (for cytoplasm) and nucleolin (for nucleus) were used as internal controls. Quantitative data was analysed using ImageJ software. Results are expressed as the mean ± SD of three separate experiments. $*p < 0.05$, $**p < 0.01$ vs. the PM treated group or $^\#p < 0.05$, $^{\#\#}p < 0.01$ vs. the un-stimulated group.
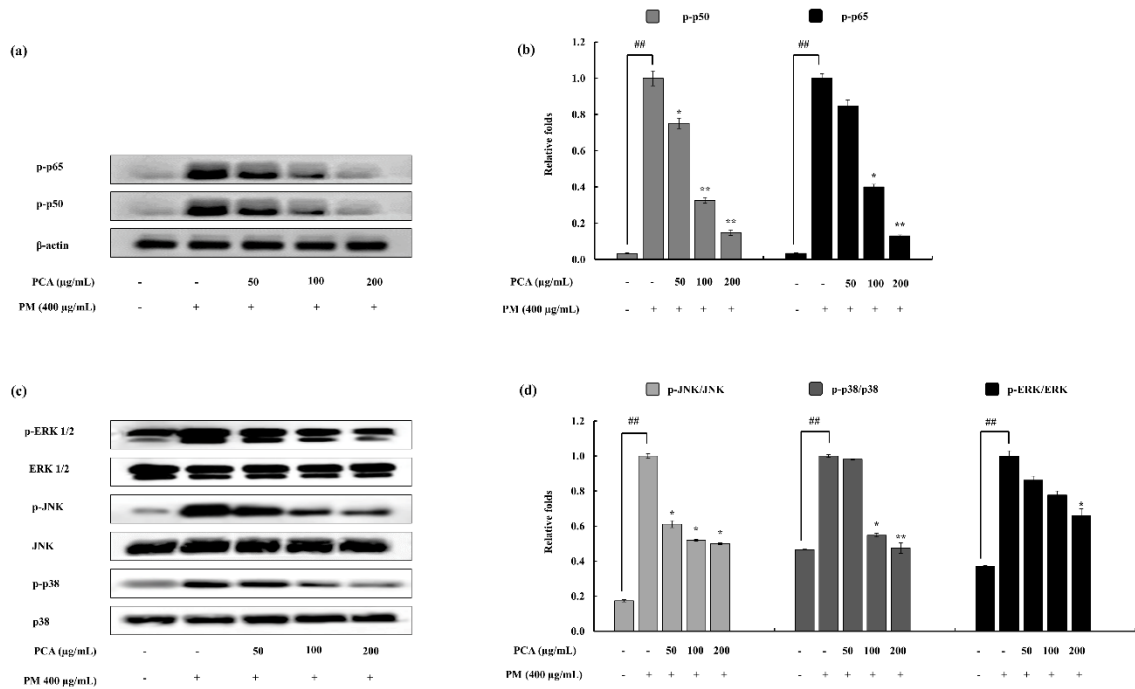
Figure 2. 9. PM induced HDF cells and co-treatment with PCA. (a) p50 and p65 in cytosol, (b) quantitative data, (c) p38, JNK and ERK, and relevant (d) quantitative data determined using western blotting. Quantitative data was analysed using ImageJ software. Results are expressed as the mean ± SD of three separate experiments. $*p < 0.05$, $**p < 0.01$ vs. the PM treated group or $^{\#}p < 0.05$, $^{\#\#}p < 0.01$ vs. the un-stimulated group.

2.3.5 Keratinocytes stimulated with PM and treated with PCA; compositional analysis

To analyse the metal ion composition of the samples which were treated with PCA, following stimulation of keratinocytes with PM, ICP-OES was used. Several metal ions including Mg, Al, K, Ca, Fe, Mn, Cu, Sr, Ba, and Pb were observed to be significantly increased in the PM treated group (Table 2.3). The record highest was Pb while Cu remains the lowest. Our experiment suggested that with the treatment of PCA the metal concentrations downregulated dose-dependently. Substantial cutbacks were observed in Pb and Cu, followed by Sr, Ba, and Mg. The graphical representation of alginate polymer and formation of the egg-box model in metal chelation is represented in the Figure 2.10.
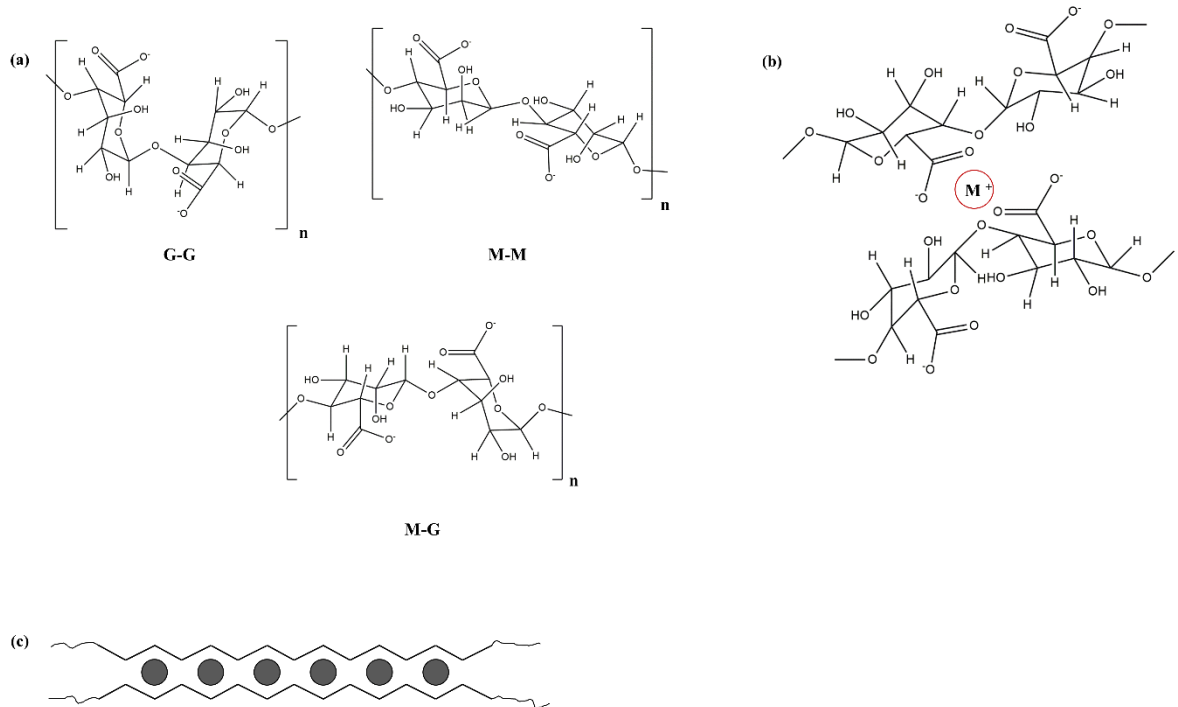
Figure 2. 10. Distribution of respective blocks of alginates. (a) Structure of alginic acid combining different monomeric units (G block; α-L-guluronic acid repeating units, M block; β-D-mannuronic acid repeating units, MG block; interchanging units of two acids) (b) The egg box model represented with the chemical formula of alginate units and (c) graphical representation.

Table 2. 3. Metal composition analysis of keratinocytes

	Control	PM	PM+PCA (50)	PM+PCA (100)	PM+PCA (200)
Mg	54.67 ± 1.47	128.53 ± 2.51	137.44 ± 4.97	101.46 ± 6.14	84.95 ± 2.11
Al	0.91	125.08 ± 9.1	119.33 ± 8.21	79.31 ± 5.12	56.92 ± 3.52
K	452.98 ± 14.56	437.37 ± 18.47	522.65 ± 20.22	504.28 ± 31.58	466.12 ± 19.68
Ca	224.44 ± 12.56	344.37 ± 10.45	385.24 ± 9.56	321.07 ± 5.36	256.44 ± 7.48
Fe	ND	174.50 ± 4.57	163.62 ± 6.89	106.52 ± 7.58	77.27 ± 5.23
Mn	ND	80.2 ± 2.47	68.4 ± 3.93	45.2 ± 2.42	32.1 ± 2.9
Cu	ND	20.1 ± 1.44	10.84 ± 1.89	6.53 ± 2.01	ND
Sr	0.71	42.18 ± 1.32	31.94 ± 2.58	21.37 ± 1.22	11.86 ± 1.09
Ba	ND	92.92 ± 6.33	72.56 ± 4.39	51.99 ± 3.15	20.41 ± 1.02
Pb	ND	241.74 ± 12.46	168.41 ± 14.15	102.47 ± 6.27	58.96 ± 3.68

2.4. Discussion

Particulate matter air pollution has become a major issue in recent years in the region of East Asia. Countries like Korea, Japan and China are the most affected. Recent publications propose that particulate matter exposure is associated with respiratory complications, allergic reactions and inflammatory skin conditions. This is a complex mixture of different components. It includes various dust types such as tobacco smoke, pollen, and exhaust gas from traffic emissions [88].

The present study, evaluated the physical parameters of the PM via the SEM and continued on inflammatory effects in keratinocytes and fibroblasts. Alginic acid was purified from *P. commersonii* and its ability to inhibit PM stimulated inflammation was evaluated. As indicated in Table 2. 2, the purified alginate (PCA) was consisted of comparatively high amount of polysaccharide and traceable amounts of proteins and polyphenols. This supports the efficient purification of alginate. Initially the *P. commersonii* powder was depigmented using both hexane and 95% ethanol. This ensures the removal of lipids, pigments both non-polar and polar as well as polyphenols reasonably. It is rather difficult to remove the effect of polyphenolic compounds due to its strong dipolar moments between polysaccharides. The usage of 10% formaldehyde in ethanol facilitates the formation of a phenolic polymer which in result lower the solubility of phenolic substances hence could be removed from the sample [89]. The alginic acid is present in brown seaweed prominently as calcium salt, but other forms such as magnesium, potassium and sodium salts are also available in minute amounts. In this particular method, the alginates in the seaweed are converted into soluble alginate via alkaline treatment. Prior to this step to increase the extraction efficacy, the sample is acid washed with dilute mineral acid (HCl). The calcium ions are exchanged with the protons and at the same time mineral acid removes the acid soluble phenolic compounds.

67

Following filtration step guarantees the removal of insoluble seaweed residues and the subsequent continuation of the sodium alginate solution. Recovering sodium alginate from this solution is not practical via evaporation due to its low concentration. Hence, the alginates can be precipitated as its calcium salt through addition of $CaCl_2$. The recovered alginates in the form of calcium alginates are then converted in to alginic acid by addition of diluted mineral acid. Finally the alginic acid is further converted into sodium alginate using NaOH and the pH is uplifted to neutral value [90]. The dialysis process removes excess ions. Alginic acid is mainly based on two monomeric units. β-D-mannuronic acid and α-L-guluronic acid which are respectively designated as M and G blocks. The polymer is formed via joining the monomers at C-1 and C-4 positions. The polymer chain is consisted of three kinds of molecules; M blocks based entirely on β-D-mannuronic acid, G blocks derived from α-L-guluronic acid, and MG blocks including interchanging units of the two acids. The proportion of the three types of blocks determine the physical properties of alginates [91-93]. Donati et al (2003), reported that the monomer sequence is possible to differ not only among different species but also in variable tissues in the same species [94].

The chemical characterization of PCA are in good argument with the sodium alginate commercial sample. The study referred several previously published data along with the analyzed data of this research. The broad peak at the 3425 cm^{-1} indicate the O-H stretching vibrations of the hydrogen bonds. The asymmetric O-C-O stretching vibrations of the carboxylate groups are represented via the 1680 cm^{-1} intense peak while symmetric vibrations are indicated via the 1420 cm^{-1} intense band. Further, weak band at the 1035 cm^{-1} assigns C-O and C-C stretching vibrations in the pyranose ring. The anomeric carbons are represented in the 750-950 cm^{-1} region [87]. The interaction

between metal ions and carboxylate groups in alginates in FTIR representation are further discussed in the report published by Papageorgiou et al. (2010) [95].

In between the external and internal environments, skin is considered to be more than a physical barrier. A crucial role of the skin is to provide immune functions. It is suggested to function as semiautonomous immunological organ. As the keratinocytes are the outermost layer of the skin, it is regularly used to assess the effect of the irritants in the dermatology. These cells participate in immune responses via the production of cytokines against the inflammatory events. This function widely contributes towards the skin to function as an immune organ. Keratinocytes can transfer stimuli into signals and successively to the other members of the skin immune system [76].

Heavy metal contamination is associated with biosoption, accumulation, and toxicity; thus has become a major concern which causes both environmental and health issues. The metal ion concentrations (Pb, Ca, Sr, Ba, and Mg) were significantly down-regulated, dose-dependently via the treatment of PCA. Earlier reports by Schaumann et al (2004), indicate that transition metal ions (Zn, Cu, and Cd) are responsible for the cause of inflammation via inducing oxidant generation. The report further illustrates that the increased concentrations of metal ions in the particulate matter contribute the oxidative stress and hence promote the activation of several transcription factors leading to discharge pro-inflammatory mediators [96]. Heavy metals can be removed from a system using vivid methods according to Wang et al (2011). One of them being chemical precipitation of metal ions using potassium/ sodiumthiocarbonate, sodiumdimethyldithiocarbamate and tri mercapto triazine. Some other methods are sulphide precipitation, adsorption, filtration using membranes and ion exchange. Further, chelation of heavy metals using biopolymers now has received much attention among the

69

scientific community [97, 98]. This follows formation of complexes between the biopolymers and the metal ions. The affinity is influenced by several factors including the structure of the polymer and ionic charge, electronic configuration, coordination number of the metal ion [99]. Alginic acid as well as its derivatives are considered as capable polysaccharides in metal chelation [100]. As alginic acid contain carboxylic groups; metal carboxylate coordination can take place. Four distinct metal-carboxylate coordination types are described by Papageorgiou et al (2010); ionic uncoordinated, unidentate coordination, bidentate chelating coordination, and bidentate bridging [95]. The structure of the alginic acid is consisted with M and G blocks; and this influences the metal ion chelation. The "egg-box" model proposed by Grant et al (1973) describes alginates prefer binding divalent cations [80, 101].

The inflammation process is regulated via a complex signaling pathways. The process possibly initiated and developed involving several pro-inflammatory cytokines. The cytokines addressed in this research were downregulated upon the PCA treatment. Among them, IL-6 indicated significant downregulation compared to others. Further, PGE_2 another inflammatory mediator was also declined. The COX-2 downregulation supported the PGE_2 decrement as it's an enzyme involved in the generation of PGE_2 via arachidonic pathway. Downstream signals in the NF-κB and MAPK pathways were also investigated. Kim et al (2014), addresses these signals as important regulators in inflammation studies focusing on the cytokine induced keratinocytes and skin. It reports the inhibition of JAK/STAT, NF-κB and PI3K/Akt signaling resulting in pro-inflammatory mediator, enzyme, cytokine and chemokine inhibition [102]. The NF-κB dimers are residing in the cytoplasm interacting with the inhibitory proteins, IκBs. With the stimulation mainly due to pro-inflammatory cytokines, the IκB kinase (IKK) is activated and phosphorylation initiates (p50 and p65). Hence, these are translocated to

70

the nucleus to activate gene transcription. IKK is a complex formed from three distinct subunits with different functions; IKKα, IKKβ, and IKKγ. Among these IKKβ is essential in NF-κB activation while IKKα involves in the signal development process [103]. The present study indicated a significant downstream in the NF-κB associated signals confirming the effect of PCA against the stimulation of PM. Similarly, MAPK signals were also down-regulated convincing the potential of PCA against PM. MAPKs play an important role in inflammation via activating pro-inflammatory cytokines and chemokines [32, 104]. These are a family of serine/threonine protein kinases which mediate biological processes in response to external stress signals. Out of three main MAPKs (p38, JNK, and ERK), p38 MAPK signals are especially involved in the regulation of the synthesis of inflammatory regulators. These factors make MAPKs a potential target in anti-inflammatory therapeutics [60].

2.5. Conclusions

The anti-inflammatory effects of alginic acid purified from *P. commersonii* is evident in this research. The particulate matter induced inflammation in keratinocytes as well as fibroblasts were inhibited via the activity of PCA. Even though it requires further experimental confirmation, the researchers believe the inflammation was highly encouraged due to the effect of heavy metal content in the PM. Hence, PCA successfully chelated the metal ions reducing its concentrations in the cell digests. Thus, PCA is applicable as a source if skin cosmetics to abate PM induced inflammation.

Acknowledgment

I would like to express my gratitude and honour to my supervisor Professor Jeon You-Jin, Head, Marine Bio-Resource Technology Lab, Department of Marine life Sciences, Jeju National University. His expertise was vital in the formulation of the research, his consistent guidance steered me through the right direction. I'm grateful to Professor Jeon for allowing me to conduct my own work and the opportunity created for me at his laboratory.

I would also like to single out Dr. Shanura Fernando whom he is my long-term colleague, who introduced me to Professor Jeon. Assistant, Associate Professors, post-doctoral positions, and lab mates are unforgettably mentioned with their dearest support towards my stay and work in the lab environment.

Finally, I must express my profound gratitude to my spouse, parents and my sibling for providing me with unfailing support throughout my years of study. This would have not been accomplished without them.

Though I have not pin pointed with names all the people who helped me, they are remembered and my gratitude is extended to them.

Thilina U. Jayawardena

References

1. Lin, Z.-C., et al., *Eupafolin nanoparticles protect HaCaT keratinocytes from particulate matter-induced inflammation and oxidative stress.* International journal of nanomedicine, 2016. **11**: p. 3907-3926.

2. Wang, W., et al., *Atmospheric particulate matter pollution during the 2008 Beijing Olympics.* Environmental Science & Technology, 2009. **43**(14): p. 5314-5320.

3. Lee, Y.G., et al., *Quiescence of Asian dust events in South Korea and Japan during 2012 spring: Dust outbreaks and transports.* Atmospheric Environment, 2015. **114**: p. 92-101.

4. Maxwell-Meier, K., et al., *Inorganic composition of fine particles in mixed mineral dust–pollution plumes observed from airborne measurements during ACE-Asia.* Journal of Geophysical Research: Atmospheres, 2004. **109**(D19).

5. Harrison, R.M. and J. Yin, *Particulate matter in the atmosphere: which particle properties are important for its effects on health?* Science of the total environment, 2000. **249**(1-3): p. 85-101.

6. Lv, B., B. Zhang, and Y. Bai, *A systematic analysis of PM2. 5 in Beijing and its sources from 2000 to 2012.* Atmospheric environment, 2016. **124**: p. 98-108.

7. Wall, S.M., W. John, and J.L. Ondo, *Measurement of aerosol size distributions for nitrate and major ionic species.* Atmospheric Environment (1967), 1988. **22**(8): p. 1649-1656.

8. Dreher, K., et al., *Soluble transition metals mediate the acute pulmonary injury and airway hyperreactivity induced by residual oil fly ash articles.* Chest, 1996. **109**(3): p. 33S-34S.

9. Kodavanti, U., et al., *Genetic variability in combustion particle-induced chronic lung injury.* American Journal of Physiology-Lung Cellular and Molecular Physiology, 1997. **272**(3): p. L521-L532.

10. Becker, S., et al., *Stimulation of human and rat alveolar macrophages by urban air particulates: effects on oxidant radical generation and cytokine production.* Toxicology and applied pharmacology, 1996. **141**(2): p. 637-648.

11. Pritchard, R.J., et al., *Oxidant generation and lung injury after particulate air pollutant exposure increase with the concentrations of associated metals.* Inhalation toxicology, 1996. **8**(5): p. 457-477.

12. Shukla, A., et al., *Inhaled particulate matter causes expression of nuclear factor (NF)-κ B–related genes and oxidant-dependent NF-κ B activation in vitro.* American journal of respiratory cell and molecular biology, 2000. **23**(2): p. 182-187.

13. Zhao, Q., et al., *Direct effects of airborne PM2.5 exposure on macrophage polarizations.* Biochimica et Biophysica Acta (BBA) - General Subjects, 2016. **1860**(12): p. 2835-2843.

14. Cho, Y.S. and H.-B. Moon, *The role of oxidative stress in the pathogenesis of asthma.* Allergy, asthma & immunology research, 2010. **2**(3): p. 183-187.

15. Bernard, K., et al., *NADPH oxidases in lung health and disease.* Antioxidants & redox signaling, 2014. **20**(17): p. 2838-2853.

16. Heo, S.-J., et al., *Evaluation of anti-inflammatory effect of fucoxanthin isolated from brown algae in lipopolysaccharide-stimulated RAW 264.7 macrophages.* Food and Chemical Toxicology, 2010. **48**(8-9): p. 2045-2051.

17. Jang, K.H., et al., *Chromenes from the Brown Alga Sargassum s iliquastrum.* Journal of natural products, 2005. **68**(5): p. 716-723.

18. Heo, S.-J., et al., *Identification of chemical structure and free radical scavenging activity of diphlorethohydroxycarmalol isolated from a brown alga, Ishige okamurae.* Journal of microbiology and biotechnology, 2008. **18**(4): p. 676-681.

19. Shanura Fernando, I.P., et al., *Antioxidant and anti-inflammatory functionality of ten Sri Lankan seaweed extracts obtained by carbohydrase assisted extraction.* Food Science and Biotechnology, 2018. **27**(6): p. 1761-1769.

20. Usoltseva, R.V., et al., *Structural characteristics and anticancer activity in vitro of fucoidan from brown alga Padina boryana.* Carbohydrate Polymers, 2018. **184**: p. 260-268.

21. Heilbron, I., R. Phipers, and H. Wright, *343. The chemistry of the algæ. Part I. The algal sterol fucosterol.* Journal of the Chemical Society (Resumed), 1934: p. 1572-1576.

22. Lee, S., et al., *Anti-oxidant activities of fucosterol from the marine algaePelvetia siliquosa.* Archives of Pharmacal Research, 2003. **26**(9): p. 719-722.

23. Jung, H.A., et al., *Anti-inflammatory activity of edible brown alga Eisenia bicyclis and its constituents fucosterol and phlorotannins in LPS-stimulated RAW264. 7 macrophages.* Food and chemical toxicology, 2013. **59**: p. 199-206.

24. Bang, M.-H., et al., *Anti-osteoporotic activities of fucosterol from sea mustard (Undaria pinnatifida).* Food Science and Biotechnology, 2011. **20**(2): p. 343.

25. Fernando, I.P.S., et al., *Beijing urban particulate matter-induced injury and inflammation in human lung epithelial cells and the protective effects of fucosterol from Sargassum binderi (Sonder ex J. Agardh).* Environmental Research, 2019. **172**: p. 150-158.

26. Fernando, I.S., et al., *Beijing urban particulate matter-induced injury and inflammation in human lung epithelial cells and the protective effects of fucosterol from Sargassum binderi (Sonder ex J. Agardh).* Environmental research, 2019. **172**: p. 150-158.

27. Fernando, I.S., et al., *3β-Hydroxy-Δ5-steroidal congeners from a column fraction of Dendronephthya puetteri attenuate LPS-induced inflammatory responses in RAW 264.7 macrophages and zebrafish embryo model.* RSC Advances, 2018. **8**(33): p. 18626-18634.

28. Suttiarporn, P., et al., *Structures of phytosterols and triterpenoids with potential anti-cancer activity in bran of black non‐glutinous rice.* Nutrients, 2015. **7**(3): p. 1672-1687.

29. Mosmann, T., *Rapid colorimetric assay for cellular growth and survival: application to proliferation and cytotoxicity assays.* Journal of immunological methods, 1983. **65**(1-2): p. 55-63.

30. Wijesinghe, W., et al., *5 [Beta]-Hydroxypalisadin B isolated from red alga Laurencia snackeyi attenuates inflammatory response in lipopolysaccharide-stimulated RAW 264.7 macrophages.* Algae, 2014. **29**(4): p. 333-341.

31. Jayawardena, T.U., et al., *Sargassum horneri (Turner) C. Agardh ethanol extract inhibits the fine dust inflammation response via activating Nrf2/HO-1 signaling in RAW 264.7 cells.* BMC complementary and alternative medicine, 2018. **18**(1): p. 249.

32. Sanjeewa, K.K.A., et al., *Ethanol extract separated from Sargassum horneri (Turner) abate LPS-induced inflammation in RAW 264.7 macrophages.* Fisheries and Aquatic Sciences, 2019. **22**(1): p. 6.

33. Livak, K.J. and T.D. Schmittgen, *Analysis of relative gene expression data using real-time quantitative PCR and the 2− ΔΔCT method.* methods, 2001. **25**(4): p. 402-408.

34. Mori, I., et al., *Development and certification of the new NIES CRM 28: urban aerosols for the determination of multielements.* Analytical and bioanalytical chemistry, 2008. **391**(6): p. 1997-2003.

35. Jeong, G.-S., et al., *Protective effect of sauchinone by upregulating heme oxygenase-1 via the P38 MAPK and Nrf2/ARE pathways in HepG2 cells.* Planta medica, 2010. **76**(01): p. 41-47.

36. Kinney, P.L., *Climate change, air quality, and human health.* American journal of preventive medicine, 2008. **35**(5): p. 459-467.

37. Brauer, M., et al., *Exposure assessment for estimation of the global burden of disease attributable to outdoor air pollution.* Environmental science & technology, 2012. **46**(2): p. 652-660.

38. Shah, A.S., et al., *Global association of air pollution and heart failure: a systematic review and meta-analysis.* The Lancet, 2013. **382**(9897): p. 1039-1048.

39. Kim, K.-H., E. Kabir, and S. Kabir, *A review on the human health impact of airborne particulate matter.* Environment International, 2015. **74**: p. 136-143.

40. Guaita, R., et al., *Short-term impact of particulate matter (PM2. 5) on respiratory mortality in Madrid.* International journal of environmental health research, 2011. **21**(4): p. 260-274.

41. Perez, L., et al., *Saharan dust, particulate matter and cause-specific mortality: a case–crossover study in Barcelona (Spain).* Environment international, 2012. **48**: p. 150-155.

42. Heo, S.-J., et al., *Antioxidant activities of enzymatic extracts from brown seaweeds.* Bioresource Technology, 2005. **96**(14): p. 1613-1623.

43. Heo, S.-J., et al., *Evaluation of anti-inflammatory effect of fucoxanthin isolated from brown algae in lipopolysaccharide-stimulated RAW 264.7 macrophages.* Food and Chemical Toxicology, 2010. **48**(8): p. 2045-2051.

44. Lee, S.-H. and Y.-J. Jeon, *Anti-diabetic effects of brown algae derived phlorotannins, marine polyphenols through diverse mechanisms.* Fitoterapia, 2013. **86**: p. 129-136.

45. Ni-Ni-Win, et al., *Three new records of Padina in Japan based on morphological and molecular markers.* Phycological Research, 2008. **56**(4): p. 288-300.

46. Sánchez-Machado, D.I., et al., *An HPLC method for the quantification of sterols in edible seaweeds.* Biomedical Chromatography, 2004. **18**(3): p. 183-190.

47. Lawrence, T., D.A. Willoughby, and D.W. Gilroy, *Anti-inflammatory lipid mediators and insights into the resolution of inflammation.* Nature Reviews Immunology, 2002. **2**(10): p. 787-795.

48. Abdul, Q.A., et al., *Health benefit of fucosterol from marine algae: a review.* Journal of the Science of Food and Agriculture, 2016. **96**(6): p. 1856-1866.

49. Alderton, W.K., C.E. Cooper, and R.G. Knowles, *Nitric oxide synthases: structure, function and inhibition.* Biochemical Journal, 2001. **357**(Pt 3): p. 593-615.

50. Jayawardena, T.U., et al., *Sargassum horneri and isolated 6-hydroxy-4,4,7a-trimethyl-5,6,7,7a-tetrahydrobenzofuran-2(4H)-one (HTT); LPS-induced inflammation attenuation via suppressing NF-κB, MAPK and oxidative stress through Nrf2/HO-1 pathways in RAW 264.7 macrophages.* Algal Research, 2019. **40**: p. 101513.

51.   Nicola, N., *Guidebook to cytokines and their receptors*. 1994: Oxford University Press.

52.   Muralidharan, S. and P. Mandrekar, *Cellular stress response and innate immune signaling: integrating pathways in host defense and inflammation.* Journal of leukocyte biology, 2013. **94**(6): p. 1167-1184.

53.   Czura, C.J., S.G. Friedman, and K.J. Tracey, *Neural inhibition of inflammation: the cholinergic anti-inflammatory pathway.* Journal of endotoxin research, 2003. **9**(6): p. 409-413.

54.   Phull, A.-R., et al., *In vitro and in vivo evaluation of anti-arthritic, antioxidant efficacy of fucoidan from Undaria pinnatifida (Harvey) Suringar.* International journal of biological macromolecules, 2017. **97**: p. 468-480.

55.   Tahir, I., et al., *Evaluation of phytochemicals, antioxidant activity and amelioration of pulmonary fibrosis with Phyllanthus emblica leaves.* BMC complementary and alternative medicine, 2016. **16**(1): p. 406.

56.   Phull, A.R. and S.J. Kim, *Fucoidan from Undaria pinnatifida regulates type II collagen and COX-2 expression via MAPK and PI3K pathways in rabbit articular chondrocytes.* Biologia, 2017. **72**(11): p. 1362-1369.

57.   Mills, E.L. and L.A. O'Neill, *Reprogramming mitochondrial metabolism in macrophages as an anti-inflammatory signal.* European journal of immunology, 2016. **46**(1): p. 13-21.

58.   Kauppinen, A., et al., *Antagonistic crosstalk between NF-κB and SIRT1 in the regulation of inflammation and metabolic disorders.* Cellular signalling, 2013. **25**(10): p. 1939-1948.

59.   Li, Q. and I.M. Verma, *NF-κB regulation in the immune system.* Nature reviews immunology, 2002. **2**(10): p. 725.

60.   Kaminska, B., *MAPK signalling pathways as molecular targets for anti-inflammatory therapy—from molecular mechanisms to therapeutic benefits.* Biochimica et Biophysica Acta (BBA) - Proteins and Proteomics, 2005. **1754**(1): p. 253-262.

61.   Tak, P.P. and G.S. Firestein, *NF-κB: a key role in inflammatory diseases.* The Journal of Clinical Investigation, 2001. **107**(1): p. 7-11.

62.   Pearson, G., et al., *Mitogen-activated protein (MAP) kinase pathways: regulation and physiological functions.* Endocrine reviews, 2001. **22**(2): p. 153-183.

63.   Raingeaud, J., et al., *MKK3- and MKK6-regulated gene expression is mediated by the p38 mitogen-activated protein kinase signal transduction pathway.* Molecular and Cellular Biology, 1996. **16**(3): p. 1247-1255.

64.   Kyriakis, J.M. and J. Avruch, *Mammalian Mitogen-Activated Protein Kinase Signal Transduction Pathways Activated by Stress and Inflammation.* Physiological Reviews, 2001. **81**(2): p. 807-869.

65.   Yoo, M.-S., et al., *Fucosterol isolated from Undaria pinnatifida inhibits lipopolysaccharide-induced production of nitric oxide and pro-inflammatory cytokines via the inactivation of nuclear factor-κB and p38 mitogen-activated protein kinase in RAW264.7 macrophages.* Food Chemistry, 2012. **135**(3): p. 967-975.

66.   Rao, K.M.K., T. Meighan, and L. Bowman, R*ole of mitogen-activated protein kinase activation in the production of inflammatory mediators: differences between primary rat alveolar macrophages and macrophage cell lines.* Journal of Toxicology and Environmental Health, Part A, 2002. **65**(10): p. 757-768.

67. Kobayashi, M., et al., *The antioxidant defense system Keap1-Nrf2 comprises a multiple sensing mechanism for responding to a wide range of chemical compounds.* Molecular and cellular biology, 2009. **29**(2): p. 493-502.

68. Canning, P., F.J. Sorrell, and A.N. Bullock, *Structural basis of Keap1 interactions with Nrf2.* Free Radical Biology and Medicine, 2015. **88**: p. 101-107.

69. Loboda, A., et al., *Heme oxygenase-1 and the vascular bed: from molecular mechanisms to therapeutic opportunities.* Antioxidants & redox signaling, 2008. **10**(10): p. 1767-1812.

70. Turnbull, A.B. and R.M. Harrison, *Major component contributions to PM10 composition in the UK atmosphere.* Atmospheric Environment, 2000. **34**(19): p. 3129-3137.

71. Fernando, I.P.S., et al., *Inhibition of inflammatory responses elicited by urban fine dust particles in keratinocytes and macrophages by diphlorethohydroxycarmalol isolated from a brown alga Ishige okamurae.* ALGAE, 2017. **32**(3): p. 261-273.

72. Gilmour, P.S., et al., *Adverse health effects of PM10 particles: involvement of iron in generation of hydroxyl radical.* Occupational and Environmental Medicine, 1996. **53**(12): p. 817-822.

73. Knaapen, A.M., et al., *Soluble metals as well as the insoluble particle fraction are involved in cellular DNA damage induced by particulate matter*, in *Oxygen/Nitrogen Radicals: Cell Injury and Disease*, V. Vallyathan, X. Shi, and V. Castranova, Editors. 2002, Springer US: Boston, MA. p. 317-326.

74. Brown, D.M., et al., *Size-Dependent Proinflammatory Effects of Ultrafine Polystyrene Particles: A Role for Surface Area and Oxidative Stress in the Enhanced Activity of Ultrafines.* Toxicology and Applied Pharmacology, 2001. **175**(3): p. 191-199.

75. Schins, R.P.F., et al., *Inflammatory effects of coarse and fine particulate matter in relation to chemical and biological constituents.* Toxicology and Applied Pharmacology, 2004. **195**(1): p. 1-11.

76. Williams, I.R. and T.S. Kupper, *Immunity at the surface: Homeostatic mechanisms of the skin immune system.* Life Sciences, 1996. **58**(18): p. 1485-1507.

77. Werner, S., et al., *Large induction of keratinocyte growth factor expression in the dermis during wound healing.* Proceedings of the National Academy of Sciences, 1992. **89**(15): p. 6896-6900.

78. Fernando, I.S., et al., *Reduction of heavy metal (Pb2+) biosorption in zebrafish model using alginic acid purified from Ecklonia cava and two of its synthetic derivatives.* International journal of biological macromolecules, 2018. **106**: p. 330-337.

79. Sarithakumari, C.H., G.L. Renju, and G.M. Kurup, *Anti-inflammatory and antioxidant potential of alginic acid isolated from the marine algae, Sargassum wightii on adjuvant-induced arthritic rats.* Inflammopharmacology, 2013. **21**(3): p. 261-268.

80. Fernando, I.P.S., et al., *Anti-inflammatory potential of alginic acid from Sargassum horneri against urban aerosol-induced inflammatory responses in keratinocytes and macrophages.* Ecotoxicology and Environmental Safety, 2018. **160**: p. 24-31.

81. Dubois, M., et al., *Colorimetric method for determination of sugars and related substances.* Analytical chemistry, 1956. **28**(3): p. 350-356.

82. Chandler, S. and J. Dodds, *The effect of phosphate, nitrogen and sucrose on the production of phenolics and solasodine in callus cultures of Solanum laciniatum.* Plant Cell Reports, 1983. **2**(4): p. 205-208.

83. Cardenas-Jiron, G., et al., *Vibrational spectroscopy and density functional theory calculations of poly-D-mannuronate and heteropolymeric fractions from sodium alginate.* Journal of Raman Spectroscopy, 2011. **42**(4): p. 870-878.

84. Wang, L., et al., *Protective effect of gallic acid derivatives from the freshwater green alga Spirogyra sp. against ultraviolet B-induced apoptosis through reactive oxygen species clearance in human keratinocytes and zebrafish.* Algae, 2017. **32**(4): p. 379-388.

85. Lee, S.-H., et al., *Cellular activities and docking studies of eckol isolated from Ecklonia cava (Laminariales, Phaeophyceae) as potential tyrosinase inhibitor.* Algae, 2015. **30**(2): p. 163-170.

86. Kim, S.-Y., et al., *Polyphenol-rich fraction from Ecklonia cava (a brown alga) processing by-product reduces LPS-induced inflammation in vitro and in vivo in a zebrafish model.* Algae, 2014. **29**(2): p. 165-174.

87. Fertah, M., et al., *Extraction and characterization of sodium alginate from Moroccan Laminaria digitata brown seaweed.* Arabian Journal of Chemistry, 2017. **10**: p. S3707-S3714.

88. Kim, K.E., D. Cho, and H.J. Park, *Air pollution and skin diseases: adverse effects of airborne particulate matter on various skin diseases.* Life sciences, 2016. **152**: p. 126-134.

89. Hahn, T., et al., *Novel procedures for the extraction of fucoidan from brown algae.* Process biochemistry, 2012. **47**(12): p. 1691-1698.

90. McHugh, D.J., *Production, properties and uses of alginates.* Production and Utilization of Products from Commercial Seaweeds. FAO. Fish. Tech. Pap, 1987. **288**: p. 58-115.

91. Smidsrod, O. and A. Haug, *Dependence upon the gel-sol state of the ion-exchange properties of alginates.* Acta chem. scand, 1972. **26**(5): p. 2063-2074.

92. Penman, A. and G. Sanderson, *A method for the determination of uronic acid sequence in alginates.* Carbohydrate Research, 1972. **25**(2): p. 273-282.

93. Haug, A., B. Larsen, and O. Smidsrød, *Uronic acid sequence in alginate from different sources.* Carbohydrate Research, 1974. **32**(2): p. 217-225.

94. Donati, I., et al., *Galactose-substituted alginate: Preliminary characterization and study of gelling properties.* Biomacromolecules, 2003. **4**(3): p. 624-631.

95. Papageorgiou, S.K., et al., *Metal–carboxylate interactions in metal–alginate complexes studied with FTIR spectroscopy.* Carbohydrate Research, 2010. **345**(4): p. 469-473.

96. Schaumann, F., et al., *Metal-rich Ambient Particles (Particulate Matter2.5) Cause Airway Inflammation in Healthy Subjects.* American Journal of Respiratory and Critical Care Medicine, 2004. **170**(8): p. 898-903.

97. Fu, F. and Q. Wang, *Removal of heavy metal ions from wastewaters: A review.* Journal of Environmental Management, 2011. **92**(3): p. 407-418.

98. Blue, L.Y., et al., *Low-level mercury removal from groundwater using a synthetic chelating ligand.* Water Research, 2008. **42**(8): p. 2025-2028.

99. King, R.B., *Coordination Number, Electronic Configuration, and Ionic Charge as Discrete Variables in Coordination Chemistry.* Adv. Chem. Ser., 1967. **62**(62): p. 203-220.

100. Jeon, C., J.Y. Park, and Y.J. Yoo, *Novel immobilization of alginic acid for heavy metal removal.* Biochemical Engineering Journal, 2002. **11**(2): p. 159-166.

101. Grant, G.T., et al., *Biological interactions between polysaccharides and divalent cations: The egg-box model.* FEBS Letters, 1973. **32**(1): p. 195-198.

102. Kim, B.-H., et al., *Anti-inflammatory activity of compounds isolated from Astragalus sinicus L. in cytokine-induced keratinocytes and skin.* Experimental &Amp; Molecular Medicine, 2014. **46**: p. e87.

103. Karin, M. and M. Delhase, *The IκB kinase (IKK) and NF-κB: key elements of proinflammatory signalling.* Seminars in Immunology, 2000. **12**(1): p. 85-98.

104. Akira, S., *Toll-like Receptors and Innate Immunity*, in *Advances in Immunology*, F.J. Dixon, Editor. 2001, Academic Press. p. 1-56.